

**AN EXPERIMENTAL INVESTIGATION OF FOAM FLOW
IN HOMOGENEOUS AND HETEROGENEOUS
POROUS MEDIA**

SUPRI TR – 112 Report

**By
Osman G. Apaydin
Henri Bertin
Louis M. Castanier
Anthony R. Kavscek**

June 1998

Work Performed Under Contract No. DE-FG22-96BC14994

**Prepared for
U.S. Department of Energy
Assistant Secretary for Fossil Energy**

**Thomas Reid, Project Manager
National Petroleum Technology Office
P.O. Box 3628
Tulsa, OK 74101**

**Prepared by:
Stanford University
Stanford, California**

TABLE OF CONTENTS

List of Tables.....	iv
List of Figures.....	v
Acknowledgements.....	vii
Abstract.....	viii
1. Introduction	1
1.1. Usage of CT Scanner in Porous Media Experiments	7
2. Foamer Solution Properties	11
2.1. Chromatography Column Experiments	12
2.1.1 Experimental Setup and Procedures	12
2.1.2 Results and Discussion	15
2.2. Surface Tension Measurements.....	18

3. Homogeneous Sand-Pack Experiments.....	21
3.1. Experimental Setup and Procedures.....	21
3.2. Results and Discussion.....	27
4. Heterogeneous Pack Experiments	55
4.1. Experimental Setup and Procedures.....	56
4.2. Results and Discussion.....	62
5. Nomenclature	78
6. References	79

LIST OF TABLES

Table 1. Experimental results for the first set of experiments.....	17
Table 2. Experimental results for the second set of experiments.....	17
Table 3. Surface tension measurement results.	20
Table 4. Summary of important parameters for homogenous pack experiments.....	28

LIST OF FIGURES

Fig. 1. Experimental setup of chromatography column experiments.....	14
Fig. 2. Surface tension and pressure drop vs. surfactant concentration.....	20
Fig. 3. Experimental setup of the homogenous core experiments.....	24
Fig. 4. Porosity profile along pack 1.	25
Fig. 5. Porosity profile along pack 2.	26
Fig. 6. Water saturation profile for 0.005 wt % foamer solution.	29
Fig. 7. Cumulative water recovery curve for 0.005 wt % foamer solution.	30
Fig. 8. Measured absolute pressure data along the core for 0.005 wt % foamer solution.	31
Fig. 9. Pressure drop data along the core for 0.005 wt % foamer solution.	32
Fig. 10. Water saturation profile for 0.01 wt % foamer solution.	35

Fig. 11. Cumulative water recovery curve for 0.01 wt % foamer solution.	36
Fig. 12. Measured absolute pressure data along the core for 0.01 wt % foamer solution.	37
Fig. 13. Pressure drop data along the core for 0.01 wt % foamer solution.	38
Fig. 14. Water saturation profile for 0.02 wt % foamer solution.	40
Fig. 15. Cumulative water recovery curve for 0.02 wt % foamer solution.	41
Fig. 16. Measured absolute pressure data along the core for 0.02 wt % foamer solution.	42
Fig. 17. Pressure drop data along the core for 0.02 wt % foamer solution.	43
Fig. 18. Water saturation profile for 0.1 wt % foamer solution.	45
Fig. 19. Measured absolute pressure data along the core for 0.1 wt % foamer solution.	46
Fig. 20. Pressure drop data along the core for 0.1 wt % foamer solution.	47
Fig. 21. Water saturation profile for 1.0 wt % foamer solution.	49
Fig. 22. Cumulative water recovery curve for 1.0 wt % foamer solution.	50
Fig. 23. Measured absolute pressure data along the core for 1.0 wt % foamer solution.	51
Fig. 24. Pressure drop data along the core for 1.0 wt % foamer solution.	52
Fig. 25. Three-dimensional reconstruction of porosity field of heterogeneous core.	57
Fig. 26. Axial porosity profile obtained with X-ray CT scanning.	58
Fig. 27. Configuration of heterogeneous porous medium during experiments. Gas is injected at the left face.	61

Fig. 28. Transient aqueous phase saturation profiles for gas-only displacement with crossflow: (a) sandstone and (b) sand regions. Heterogeneous side injection. ...	63
Fig. 29. Transient aqueous phase saturation profiles for gas-only displacement without crossflow: (a) sandstone and (b) sand regions. Homogenous side injection.	64
Fig. 30. Water saturation profiles in the heterogeneous core section, $t = 0.23$ PV. Cross flow is not permitted. Heterogeneous side injection	66
Fig. 31. Transient aqueous phase saturation profiles for displacement without crossflow: (a) sandstone and (b) sand regions. Heterogeneous side injection. .	67
Fig. 32. Transient aqueous phase saturation profiles for displacement with crossflow: (a) sandstone and (b) sand regions. Heterogeneous side injection.	70
Fig. 33. Transient aqueous phase saturation profiles for displacement without crossflow: (a) sandstone and (b) sand regions. Homogeneous side injection. .	72
Fig. 34. Transient aqueous phase saturation profiles for displacement with crossflow: (a) sandstone and (b) sand regions. Homogeneous side injection. ..	74

ACKNOWLEDGMENTS

This work was supported by the U.S. Department of Energy under Contract No. DE-FG22-96BC14994 to Stanford University. Likewise, the support of the SUPRI-A Industrial Affiliates is acknowledged.

ABSTRACT

Foam is used to reduce the high mobility of gas-drive fluids and improve the contact between oil and these injected fluids. We require a better understanding of the effect of surfactant concentration on foam flow in porous media. Besides this, the literature on foam flow and transport in heterogeneous systems is sparse although the field situation is primarily heterogeneous and multidimensional. In this study, foam flow experiments were conducted first in homogenous sand packs to investigate the effect of surfactant concentration on foam flow and then a heterogeneous experimental setup was prepared to observe heterogeneity and multidimensional flow effects on foam propagation.

The homogeneous core experiments were conducted in a cylindrical aluminum core holder that was packed with a uniform Ottawa sand. Sand permeability is about 7.0 Darcy. The experiments were interpreted in terms of evolution of in-situ water saturation as a function of time by the usage of CT scanner, cumulative water recovery, and pressure drop across the core. At very low surfactant concentration, no significant benefit was

observed. But when stable foam generation started sweep efficiency (water recovery), breakthrough time, and pressure drop increased as surfactant concentration increased.

At the next stage, a Fontainebleau sandstone was centered inside an acrylic tube and the annular region was packed with clean Ottawa sand to construct a heterogeneous porous medium. The permeability contrast between sandstone and sand was 67 to 1. Experiments with and without crossflow between the two porous media were conducted. To prevent crossflow, a heat-shrink Teflon jacket was placed on the cylindrical face of sandstone. In-situ water saturation distribution was garnered using the CT scanner. The results from this study are striking. When the heterogeneous layers were in capillary communication and cross flow was allowed, foam fronts move at identical rates in each porous medium as quantified by the CT-scan images. Desaturation by foam was efficient and typically complete in about 1 PV of gas injection. When cross flow was prohibited, foam partially plugs the high permeability sand and diverted flow into the low permeability sandstone. The foam front moved through the low permeability region faster than in the high permeability region.

CHAPTER 1

INTRODUCTION

The decreasing trend of discovery of new oil reservoirs coupled with the expanding world wide demand for energy, increases the importance of and potential for enhanced oil recovery (EOR) processes. Likewise, oil reservoir recovery efficiency is, generally, low, creating a large target of unrecovered oil. Gas drives are a common means of improving oil recovery. Fluids that are used in gas drives such as carbon dioxide, steam, enriched hydrocarbons and nitrogen have high mobility compared to water and oil because they are less viscous and are less dense compared to the fluid originally in the reservoir. These two characteristics lead gas drive fluids to channel through high permeability zones, and to rise to the top of the reservoir by gravity segregation where they override the oil. As a result sweep efficiency decreases and the amount of oil left behind increases.

Foam is suggested by many investigators to overcome the mobility problem of gas-drive fluids and improve the contact between oil and these injected fluids. Foams are

usually formed by non-wetting gases such as steam, carbon dioxide (CO₂), or nitrogen (N₂) dispersed within a continuous surfactant-laden liquid phase either by alternating (i.e. slug) injection or by co-injection of gas and surfactant solution into the reservoir. Bond and Holbrook (1958) first introduced foam in porous media to the literature and suggested that if foam is generated by consecutive injection of surfactant solution and gas into reservoirs, it improves the sweep efficiency; and Fried (1961) showed that foam reduces the gas-oil mobility ratio and acts as a gas-blocking agent. Since then, the rheology and flow mechanism of foam as well as modes of foam generation and destruction have been investigated by many researchers.

Typical field applications include aqueous foams for improving steam-drive (Patzek and Koinis, 1990; Djabbarah *et al*, 1990; Mohammadi *et al*, 1989) and CO₂-flood performance (Hoefner *et al*, 1994), gelled-foams for plugging high permeability channels (Friedman *et al*, 1997), foams for prevention or delay of gas or water coning (Aarra *et al*, 1996), and surfactant-alternating-gas processes for clean up of ground-water aquifers (Hirasaki *et al*, 1997; Hirasaki *et al*, 1997). All of these methods have been tested in both the laboratory and the field. During these processes, the gas phase is generally discontinuous and the liquid phase is continuous.

Foam changes gas mobility in two ways. The first mechanism is associated with moving bubbles and rearrangement of bubble interfacial area. Confined foam bubbles transport as bubble trains in gas-occupied channels. Gas bubbles must slide over lubricating liquid films (Bretherton, 1961). Hirasaki and Lawson (1985) studied bubble and lamellae trains. They used cylindrical capillary tubes for their experiments and

showed that during flow the front bubble interface expands in the direction of the capillary wall while the rear interface contracts in the direction of capillary centerline. Surfactant depletes at the front and accumulates at the rear of a moving bubble. This process increases the surface-tension gradient and slows the bubble motion and so increases the effective viscosity. Of course, this process requires multiple stable lamellae and disconnected gas bubbles. This stability is ensured by a disjoining pressure in the lamella between two foam bubbles. Aronson *et al* (1994) measured single film disjoining pressure and showed that it is directly dependent on the concentration of surfactants and salt that are used for foam flow in porous media. Khatib *et al* (1988) first suggested that foam film strength was directly related to gas mobility in the presence of foam.

As a second mechanism, gas mobility is decreased because foam is trapped. Gas, as a flowing foam, tends to flow through the high permeability and high porosity zones. The wetting phase occupies the smallest pore channels. Thus, trapping occurs in the intermediate-sized pores (Kovscek and Radke, 1994). Friedmann *et al* (1991) showed that at constant fractional flow, the fraction of trapped gas changed slightly as a function of gas velocity. Gillis and Radke (1990) using sulfur hexafluoride and methane simultaneously as tracers, reported that there was no consistent trend of trapped fraction with liquid or gas velocity. When they injected gas into the Berea sandstone core, they observed that 85-99 % of the gas the remained was stationary.

During the flow of gas in the reservoir, where the wetting phase is aqueous surfactant solution, foam generation and coalescence occurs continuously. Snap-off is the most significant mechanism of foam formation (Kovscek and Radke, 1994). It is a

mechanical process that occurs continuously for multiphase flow in the reservoir, regardless of the presence of surfactant. As gas flows through the reservoir pores, when it reaches a throat that is initially filled with wetting fluid, capillary pressure and curvature increase to the entry value. When the front of the interface proceeds and enters the pore space, wetting fluid remains in the corners and local capillary pressure at the gas front decreases with the expansion. This leads to a pressure gradient in the wetting fluid between the pore throat and body. Liquid flows to the throat and separates the gas to form a gas bubble. If the wetting fluid is surfactant and the suction capillary pressure is sufficient to drain a lens, then a lamella forms (Kovscek and Radke, 1994). Surfactant stabilizes the thin surfactant films between ‘bubbles. Disjoining pressure exerted between the interfaces of two gas bubbles keeps them apart.

Foam coalescence occurs by a stretching and squeezing process. While foam is flowing through pores and throats it expands and compresses simultaneously. Surfactant thin films (lamellae) separating the bubbles also stretch and squeeze by the movement of foam. When these thin films break, foam coalescence occurs. The strength of these lamellae depends on the capillary pressure and disjoining pressure, which are directly related to concentrations of surfactant and salt.

Changes in surfactant concentration have a significant effect on foam longevity in porous media. Chiang *et al* (1980) showed that foam generation generally increases with increasing surfactant concentration until the critical micelle concentration (CMC) is reached, and changing surfactant concentration has little effect above the CMC.

Likewise, Marsden and Khan (1966) found that the apparent viscosity increases with increasing surfactant concentration.

With these results in mind, we conducted a study to characterize our foamer solution before we started experiments. The screening procedure was two pronged. First, the pressure drop across a small chromatography column, packed with sand, was measured for increasing surfactant concentrations for a variety of brines. Next, the interfacial tension between air and surfactant solution was measured for increasing concentration of surfactant using pendant drop method. A broad range of surfactant concentrations was used in order to identify the CMC. We report further on the characterization procedure in Chapter 2.

Beyond these observations, it is important to determine the optimum concentration of surfactant that should be used to form foam for field applications. The amount of surfactant required has a direct effect on the economics of a project. Also, foam displacement processes within reservoirs are inherently transient. Although a fixed surfactant concentration is usually injected, transient characteristics dominate foam flow during a significant portion of the project life. We require an understanding of how the reservoir responds with changing surfactant concentration. For this purpose, we conducted foam flow experiments in a cylindrical homogenous porous medium. An aluminum core holder is packed with a uniform sand, a CT scanner is used to interpret the experiments in terms of the evolution of in-situ water saturation as a function of time, and a seven-way valve and a pressure transducer is used to obtain the absolute pressure data along the core at different locations.

The next stage of the research explored foam generation and transport in heterogeneous porous media. One can notice that, while much work has been done in homogeneous systems, the literature on flow in stratified systems is sparse. Notable experiments in stratified systems include Casteel and Djabbarah (1988) who performed steam and CO₂ displacements with foaming agents in two parallel porous media. Robin (1987) studied foam generation and transport in layered beadpacks that simulated reservoir strata. In these experiments he surmised that foam blocked the high permeability layer. Llave *et al* (1990) observed that foam can divert gas flow from high permeability layers to low permeability layers when the layers are isolated. More recently, Hirasaki *et al* (1997) performed foam displacements in layered porous media to study the removal of organic liquids from groundwater aquifers. Gas was injected at a fixed pressure gradient rather than a specified rate. By dyeing the various fluids, they observed displacement patterns directly. They found that injection of gas slugs into a porous medium containing surfactant resulted in foam generation and selective mobility reduction in the high-permeability layers. In turn, recovery of the organic liquid was greatly enhanced.

For the most part, the effect of flow among parallel layers in capillary communication has not been investigated. We denote this as cross flow. To bridge this gap, we performed additional foam flow experiments in an axially symmetric, cylindrical, heterogeneous porous medium. The central portion of the porous medium is a Fontainebleau sandstone core and a uniform sand is packed in the annular region between the core and the pressure vessel wall to complete the porous medium. By the use or absence of a heat-shrink Teflon jacket around the sandstone, fluid communication, or cross-flow, is prohibited or allowed. The sandstone is about two orders of magnitude less

permeable than the sand to provide a strong permeability and capillary pressure contrast. We interpreted the experiments in terms of the evolution of in-situ water saturation as a function of time.

In the following chapters, we first discuss characterization of our foamer solution, homogenous pack experiments and heterogeneous pack experiments in detail. Since X-ray CT scanning is our primary experimental tool, we give a brief information about the CT scanner that was used during the experimental determination of water saturation and porosity via X-ray scanning.

1.1. Usage of CT Scanner in Porous Media Experiments

A fourth generation (1200 fixed detectors) PickerTM 1200 SX X-ray scanner is used to determine porosity and water saturation distribution along the core by measuring the attenuation of a collimated beam of X-rays. We made scans perpendicular to the axis of the core to obtain images of the cross-sectional distribution of gaseous and aqueous phases in sand and sand stone as a function of time.

An X-ray source and an array of crystal detectors are needed to obtain a CT slice. When a body is placed between source and detectors, some amount of the photons are absorbed by the body and the rest of the photons reach and fluoresce the detectors. The values read at the detectors give us the beam attenuation of the body placed in the path of X-rays. The source moves around the body in a circular path and the detectors are read at small rotational intervals. The total data obtained during this process is called a slice.

After a slice is formed and stored in the computer a cross sectional image or matrix of attenuation coefficient $\mu(x,y)$ is created. The basic unit used for image reconstruction from the data is the volume element or voxel. A given CT image is formed by many voxels where each voxel has its own attenuation and is displayed as a 2-D image matrix of pixels (picture elements). A practical scale of attenuation is used based on the international unit of Hounsfield (H or CT number). Each CT unit corresponds to about a 0.1% change in the attenuation coefficient. In this scale, water and air have values of 0 and -1000 consecutively. The CT number is defined as:

$$N_{CT} = \frac{\mu_X - \mu_{WATER}}{\mu_{WATER}} \quad 1.1$$

where μ_X is the measured X-ray attenuation coefficient (Gargal 1996). X-ray CT provides accurate resolution of the progress of displacement fronts as well as the in-situ displacement efficiency. For water saturation determination at a given location, current and wet CT images, wetting phase and gas CT numbers, and porosity are needed.

In equation form:

$$N_{CTMEAS} = (1 - f)N_{CTMATRIX} + f(S_g N_{CTGAS} + S_w N_{CTWETPHASE}) \quad 1.2$$

$$N_{CTWET} = (1 - f)N_{CTMATRIX} + fN_{CTWETPHASE} \quad 1.3$$

where, N

measurement accuracy depends on the different parameters chosen for the X-ray emitter such as voltage and intensity, filters, and reproducibility of the positioning system moving the coreholder apparatus into and out of the gantry. A theoretical computation of the measurement accuracy, assuming no error in the positioning system, provides an error of 6% (Burger, J., 1996).

FOAMER SOLUTION PROPERTIES

As noted previously, foam stability generally increases with increasing surfactant concentration until the critical micelle concentration (CMC) is reached, and changing surfactant concentration has little effect on foam stability above the CMC (Chiang *et al* 1980). This is a very important property of foam as excess usage of surfactant may be prevented if the CMC is known as a function of brine properties. This may reduce the process costs. For this study, characterizing and understanding the properties of the foamer solution had great importance. We used the results of foamer characterization analysis in the evaluation of homogenous sand-pack experiments, in the interpretation of weak and strong surfactant generation, and to choose the surfactant concentration that we should use to generate strong foam during the heterogeneous pack experiments.

We conducted a two-step study to characterize our foamer solution. First, we measured pressure drop across a small chromatography column, packed with sand, for increasing surfactant concentrations for a variety of brines. Next, we measured the

interfacial tension between air and surfactant solution for increasing concentration of surfactant using the pendant drop method. A broad range of surfactant concentrations was used in order to identify the CMC. In the next two sections, we detail first the small chromatography column experiments and then surface tension measurements and results.

2.1 Chromatography Column Experiments

2.1.1 Experimental Setup and Procedures

In chromatography column experiments, a 10 cm long chromatography column (glass tube) with a 10 mm inner diameter was packed with dry sand in an upright position. The sand used in the sand pack was 100-120 mesh Ottawa sand. To ensure good settling, pneumatic vibrators were used while packing the tube. During surfactant solution injection, a DuPont Instruments Chromatographic pump (Model 861001-901) was used. A Matheson mass flow meter (0-10 sccm, Model 8240) was used to inject the gas at a constant rate. Foam was generated during co-injection of nitrogen and surfactant solution.

A Grove Mity-Mite (Model S-91LW) back-pressure regulator was used to maintain constant back pressure around 100 psi during the experiments. Because there is compressible fluid in the system (nitrogen), the back-pressure regulator showed some fluctuations, up to 10 psi, during the experiments. Fortunately this did not effect the pressure measurements hence our concern was not absolute pressure data but pressure drop data.

A differential pressure transducer (Validyne Model DP15) is used to measure the pressure drop across the chromatography tube. The pressure transducer is calibrated to 25 psi and 300 psi depending on the experiment and connected to a transducer modulator. Electrical signals obtained from the transducer modulator were then transferred to a voltmeter. Transducer was calibrated, and the transducer demodulators were adjusted before each experiment by using a voltmeter. A schematic of the experimental system is given by Fig. 1.

The surfactant used for the experiments was Shell AOS C14-16. Table salt (NaCl) was used to form the surfactant solutions, because it does not contain trace amounts of organic solvents. For the foam experiments, surfactant solutions were prepared with different concentrations: 0.0, 0.001, 0.005, 0.01, 0.02, 0.05, 0.1 and 0.5 wt %.

Porosity and permeability of the porous medium was not measured but the typical values for 100-120 mesh Ottawa sand are around 35 % porosity and 7.0 darcy permeability. Before each experiment, the porous media was saturated with surfactant solution. To reach 100 % solution saturation, several pore volumes were injected. Any gas that accumulated within the connection tubes between the sand pack and transducer was purged. System pressure was increased to 100 psi by the usage of back pressure regulator and this was followed by co-injection of nitrogen and surfactant solution.

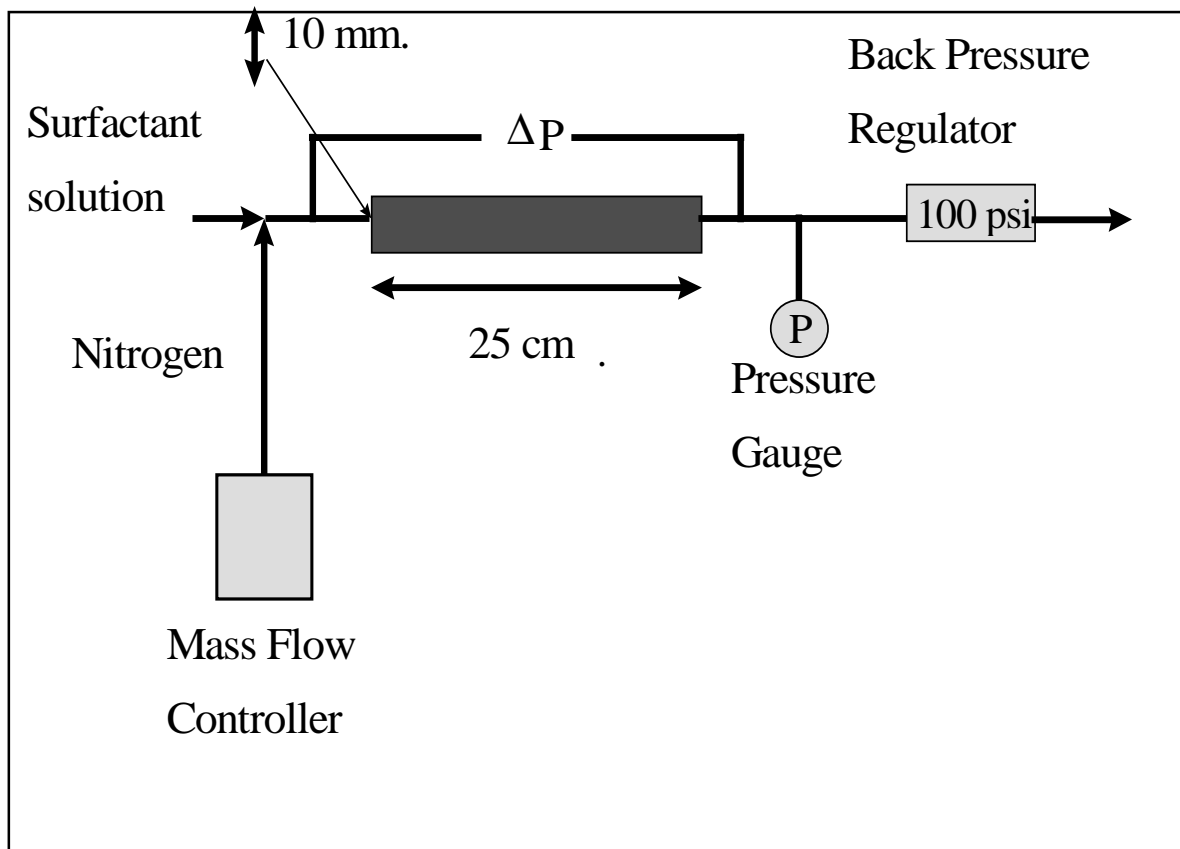


Fig. 1. Experimental setup of chromatography column experiments.

During the experiment only pressure drop data was collected and the experiment was stopped when steady state was reached.

Surfactant Concentration, wt %	Salt Concentration, wt %	Transducer Calibration, psi	Pressure Drop, psi
0.000	0.5000	25	1.5
0.001	0.0005	25	1.5
0.005	0.0025	25	1.6
*0.010	0.0050	25	4.2
*0.020	0.0100	25	>30
0.050	0.0250	300	204.0
0.100	0.0500	300	214.5
0.500	0.2500	300	200.2

Table 1. Experimental results for the first set of experiments

- Steady state had not been reached when the experiment was stopped.

Surfactant Concentration, wt %	Salt Concentration, wt %	Transducer Calibration, psi	Pressure Drop, psi
0.000	0.5	25	1.500
0.001	0.5	25	2.125
0.005	0.5	25	3.125
*0.010	0.5	300	210.00
**0.020	0.5	300	198.00
0.050	0.5	300	235.50
0.100	0.5	300	212.40
0.500	0.5	300	224.25

Table 2. Experimental results for the second set of experiments

- It took 12 hours to reach steady state
- ** It took 4 hours to reach steady state**

2.1.

Surface Tension Measurements

The pendant drop method was used to measure surface tensions of a variety of surfactant solutions to air. Detailed technical background about the method can be found in ‘Physical Chemistry of Surfaces’ by Adamson (1982). In this method, certain dimensions of the liquid drop is measured to obtain surface tension of a liquid in a liquid or a liquid in a gas. A micrometer was used to control the amount of flow of fluid and the size of the drop. A video camera was used to record the drops of liquid and later the digital pictures were printed on paper. After that, the widest part of the drop, D_e , was measured. Then a distance of D_e from the bottom of the drop was measured upwards at which point the diameter, D_s , was recorded. A correction factor, $1/H$, which is based on drop shape and tabulated (See Adamson), was read. Surface tension is calculated by using the formula:

$$\sigma = \frac{\Delta\rho g D_e^2}{H} \quad 2.1$$

where, σ is surface tension, $\Delta\rho$ is the density difference of the two fluids, g is the acceleration due to gravity, D_e is the widest part of the liquid drop, and $1/H$ is the tabulated correction factor.

As in the chromatographic core experiments, we started with very low aqueous surfactant concentrations and increased it gradually. A fixed amount of salt, 0.5 wt %, was used during the measurements. The foamer solutions used in the experiments and the measured surface tensions are tabulated in Table 3.

As can be seen in the table, adding surfactant to the solution decreases the surface tension drastically up to 0.005 wt % surfactant concentration (i.e., the critical micelle concentration) and then the trend in the decrease slows down. After 0.01 wt %, any increase in the surfactant concentration does not change surface tension. This gives an idea about how much surfactant should be added to the solution when surface tension is the concern. As seen here, after a certain range, increasing surfactant concentration in the system does not give significant benefit.

Finally, the results of the chromatographic core experiments (fixed salt concentration case) and surface tension measurements are combined. Figure 2 plots the results on the same graph. This figure is helpful in two ways. First of all, we now know that we can expect foam generation in the porous media after 0.005 wt % surfactant concentration. To investigate this further, homogenous sand-pack experiments were conducted beginning with 0.005 wt % as the first concentration. The results presented here were useful in the interpretation of weak to strong foam generation in the porous media. The homogenous sand-pack experiments will be detailed in the next chapter. Secondly, we chose the surfactant concentration for our heterogeneous core experiments, in which we wanted to generate strong foam, as 0.1 wt %. A strong foam generation is expected at this concentration.

Surfactant concentration, wt %	Surface Tension, mN/m
0.000	72.00
0.001	59.27
0.005	34.14
0.010	33.14
0.050	32.79
0.100	31.90
0.500	31.10
1.000	31.10

Table 3. Surface tension measurement results.

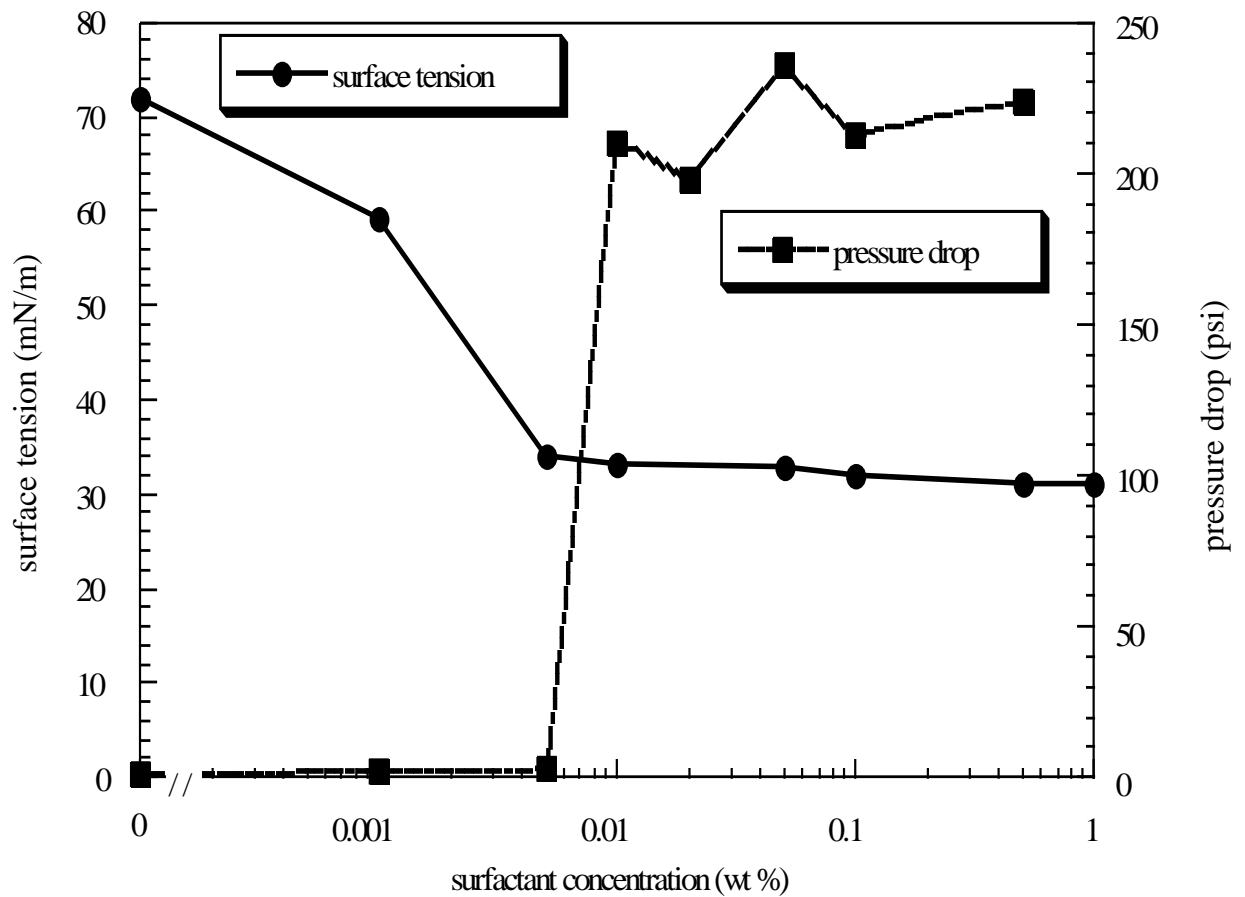


Fig. 2. Surface tension and pressure drop vs. surfactant concentration.

HOMOGENOUS SAND-PACK EXPERIMENTS

In this chapter, the effect of surfactant concentration on foam generation and transport in a cylindrical homogenous sand-pack is discussed. We require an understanding of how the recovery, pressure drop profiles, and water saturation profiles change with changing surfactant concentration. For this purpose, we conducted five foam-flow experiments using two different sand packs. In the next two sections, we detail experimental setup and procedures, and then discuss the results.

3.1 Experimental Setup and Procedures

We used a 20 in long aluminum core holder with a 2 in inner diameter. Stainless steel screens were used on each end of the sand pack to prevent sand migration. There were 6 aluminum pressure taps that were welded to the surface of the core holder. We placed Nupro 60 micron sintered filters (Swagelok, element # SS-4F-K4-60) into the pressure taps to avoid sand migration. A 6.5 mm thick, nominal 120 mesh, sintered

aluminum oxide plate was positioned at the inlet of the sand pack to aid the distribution of the injected solution, to create a permeability contrast which helps foam generation. We packed the core holder with dry 100-120 mesh Ottawa sand in an upright position. Pneumatic vibrators were used while packing to ensure good settling.

For liquid (water, foamer solution) injection purposes we used an ISCO syringe pump (Model 500 D) and an ISCO pump controller (Series D). A Matheson mass flow meter (0-10 sccm, Model 8240) was used to inject the gas (nitrogen) at a constant rate. Nitrogen and foamer solution were co-injected. Pressure responses were transmitted to a transducer through a Whitey manual 7-way valve (element # SS-43Z6). A Paroscientific pressure transducer (Model 43K-101) was assigned to measure absolute pressure values along the core. A Pentium (133 MHz) computer connected to the pressure transducer and a computer program in Visual Basic (see Appendix 1) was used to record the pressure data.

We tried to maintain constant back-pressure (around 100 psi) during the experiments using a Grove Mity-Mite (Model S-91LW) back-pressure regulator. After gas breakthrough, the back-pressure fluctuated because of the compressibility of the gas and multiphase flow in the back-pressure regulator, but this did not effect the pressure measurements because our concern was not absolute pressure data but pressure-drop data. A schematic of the experimental system is given in Fig. 3.

We used a fourth generation (1200 fixed detectors) PickerTM 1200 SX X-ray scanner to determine the porosity of the sand packs and to interpret the experiments in terms of the evolution of the in-situ water saturation as a function of time. We made

scans perpendicular to the axis of the core to obtain images of the cross-sectional distribution of gas and liquid phases in the sand at 13 locations at different times.

The surfactant used for the experiments was Shell AOS C1416. Table salt (NaCl) was used to form the surfactant solutions, because it does not contain trace amounts of organic solvents. For the foam experiments, surfactant solutions were prepared with different concentrations: 0.005, 0.01, 0.02, 0.1 and 1 wt %. Each solution had 0.5 wt % salt.

Porosity profiles of both cores were obtained using the CT scanner. Dry CT images were measured before injecting any fluid into the core (there was only air in the pore spaces), then the core was fully saturated with desired fluid (foamer solution), and wet CT images were measured to calculate porosity. Average porosity values are 35.11 and 36.22 % for pack 1 and 2, respectively. Porosity distributions along the cores can be seen in Figs. 4 and 5. As we see in the figures both of the sand packs are almost homogenous. After obtaining the porosity profiles along the core at specific locations, we started experiments and used these porosity values to calculate water saturation values at these locations. The permeability values for both sand packs were determined by injecting brine into the cores and measuring the pressure drop. The permeability values were calculated to be 6.7 and 7.0 Darcy for pack 1 and 2, respectively.

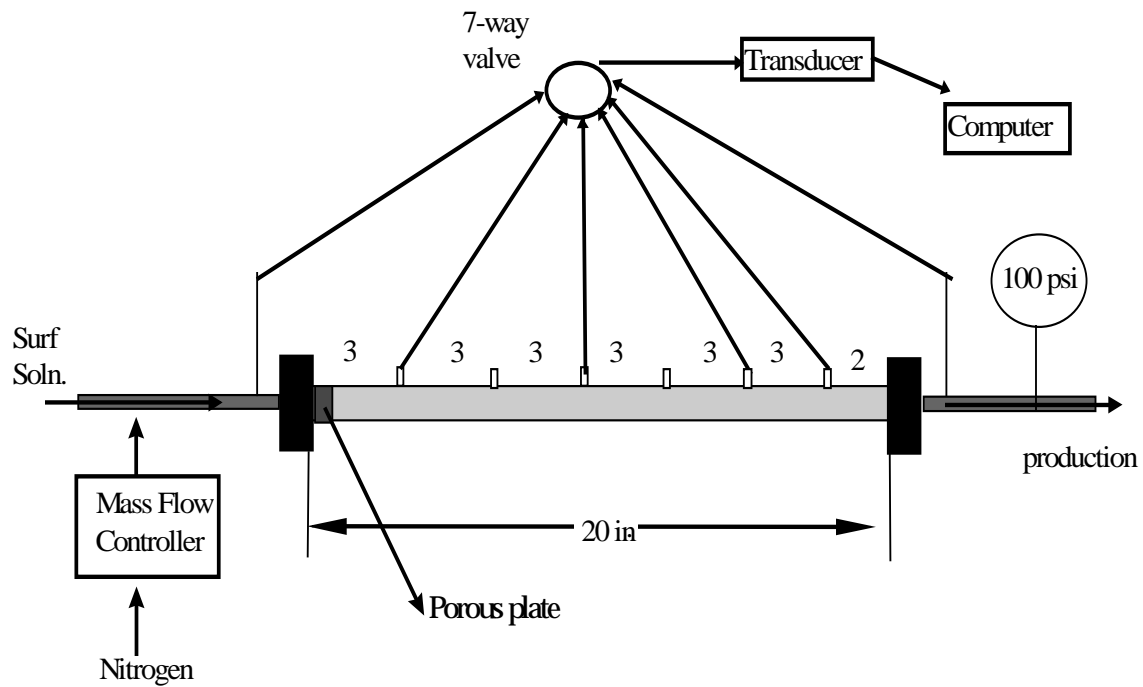


Fig. 3. Experimental setup of the homogenous core experiments.

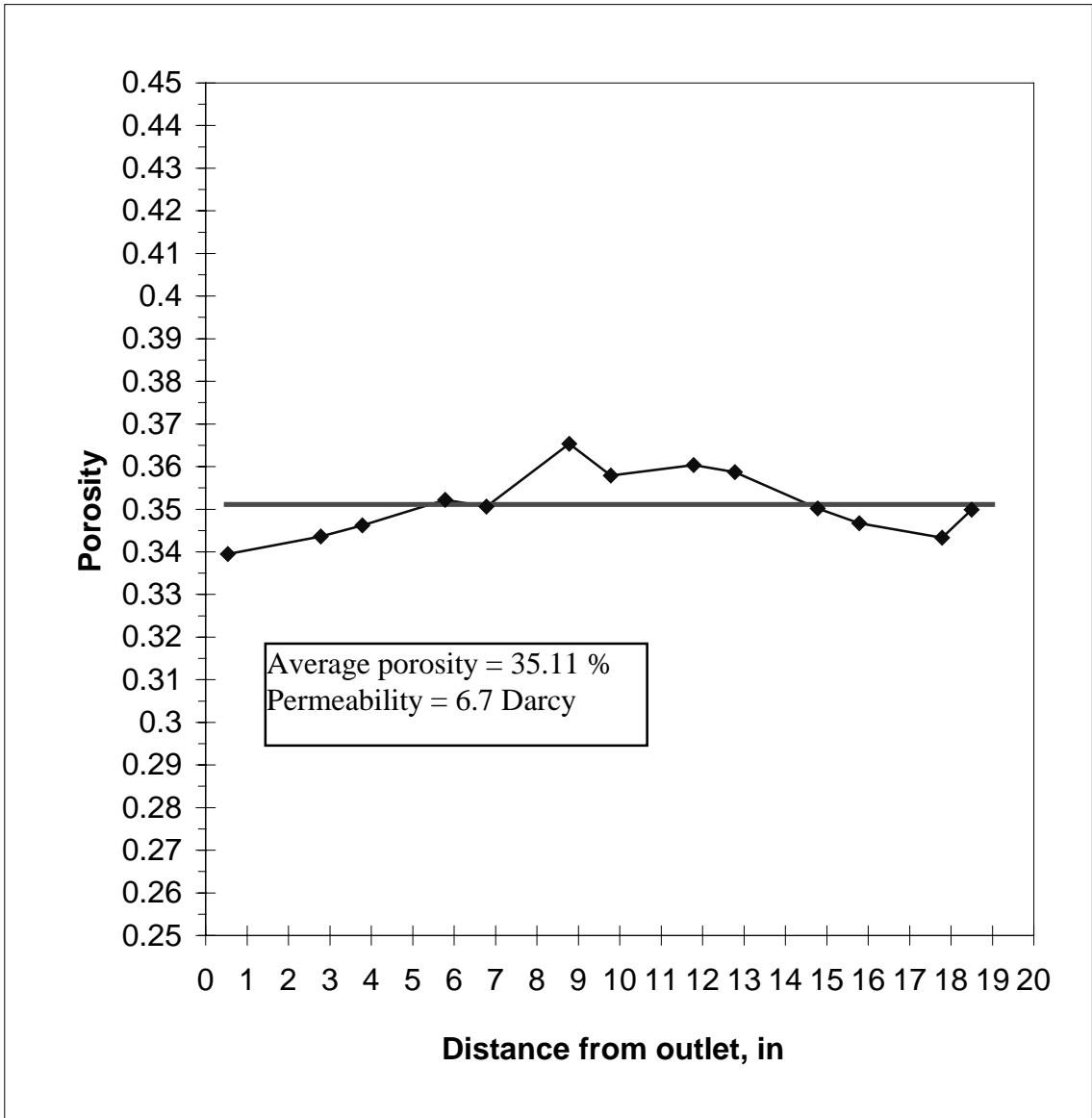


Fig. 4. Porosity profile along pack 1.

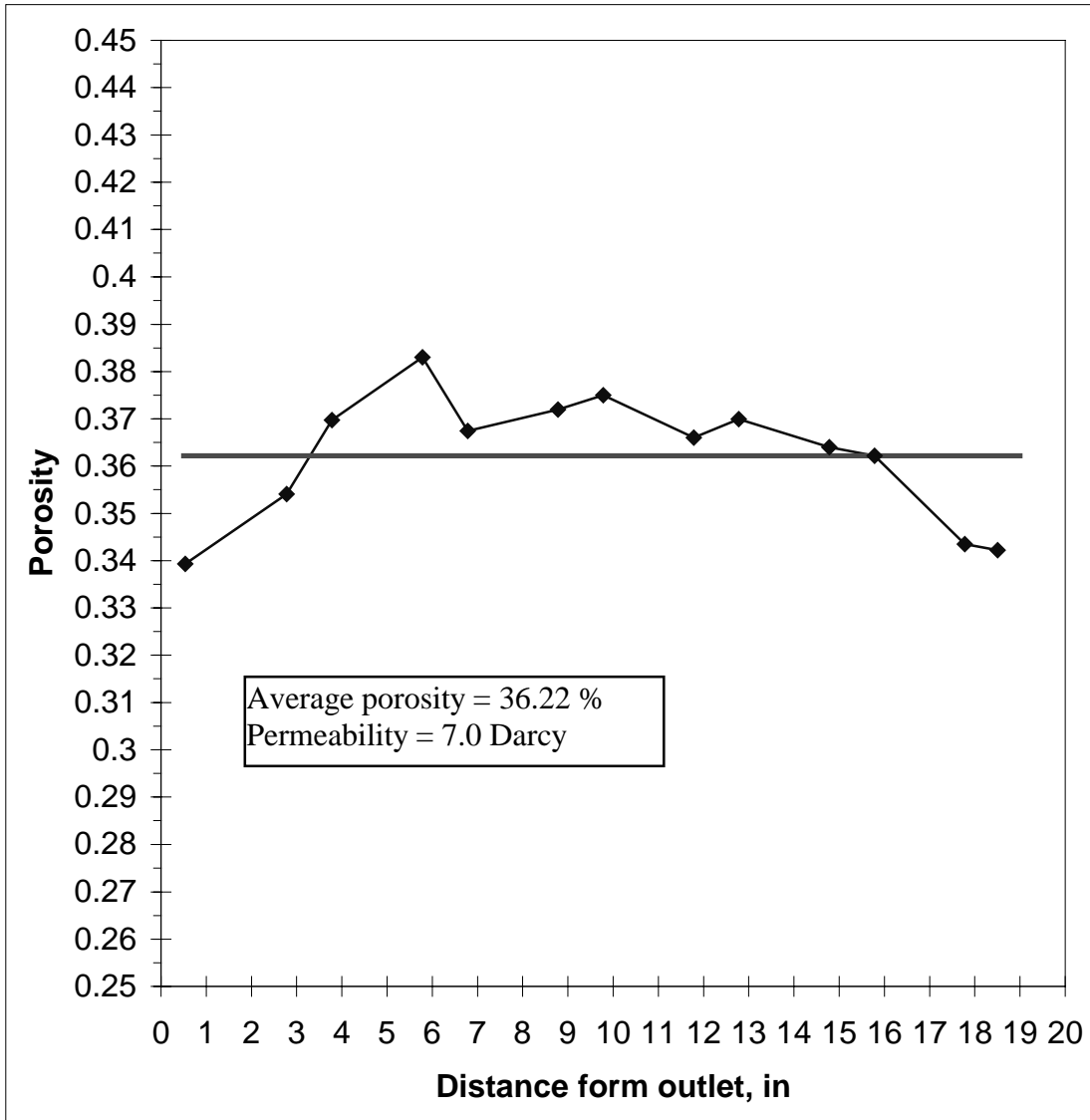


Fig. 5. Porosity profile along pack 2.

Before the first experiment, the medium, which was in a vertical position, was flushed with CO₂ from the top until it became dry. The core was fixed horizontally on the CT couch, and not moved anymore for the duration of the experiments, to avoid CT measurement errors. Dry CT scans were made at 13 locations along the core before

saturating the core to be able to calculate porosity. Then several pore volumes of foamer solution were injected until the medium was completely liquid saturated. The gas that accumulated within the connection tubes between the sand pack and transducer during CO₂ flushing was purged. System pressure was increased to 100 psi and wet CT images were measured to calculate reference water saturation data. Then co-injection of nitrogen and foamer solution followed at a constant rate. During the experiments, absolute pressure data, recovery data were measured and CT images were obtained at different times. Pressure data were collected at the inlet, outlet, and at 4 different locations along the core (Fig. 3). Co-injection continued until steady state was reached. At the end of the experiment, the core was flushed with CO₂ and the same core preparation procedure was repeated for the next experiment.

3.2.1 Results and Discussion

We employed pack 2 to conduct the 0.1 wt % foamer solution experiment and used pack 1 for the rest of the experiments. To cover the possible effect of not completely removing surfactant from the core, the experiments were started with 0.005 wt % surfactant solution and larger concentrations followed subsequently. We maintained constant back-pressure at around 100 psi. Total injection rate at this back-pressure was around 0.62 cm³/min for pack 1 experiments and it was 0.69 cm³/min for the 0.1 wt % surfactant concentration experiment, which was run in pack 2. Liquid injection rate was fixed as 0.07 cm³/min for all the experiments. Gas fractional flow was around 90 % during all the experiments. The important parameters for these runs are summarized in Table 3.

We start by discussing the low surfactant concentration results. Water saturation profiles, the recovery curve, and pressure profiles for the 0.005 wt % foamer solution experiment are given in Figs. 6-9. This experiment is performed in pack 1, where porosity is around 35 % and permeability to water is around 6.7 Darcy. Cumulative injection rate is 0.622 cm³/min (0.44 m/day superficial velocity) at 101 psi back-pressure and gas fractional flow is 87.7 %. Liquid rate is 0.07 cm³/min.

Run No.	Surfactant conc., wt %	Salt conc., wt %	Back-pressure, psi	Total injection rate, cm ³ /min	Liquid rate, cm ³ /min	Gas fractional flow, %	**Cumulative Recovery @ breakthrough, PV
1	0.005	0.5	102	0.622	0.07	87.7	0.362
2	0.01	0.5	104	0.632	0.07	88.9	0.528
3	0.02	0.5	100	0.620	0.07	88.8	0.745
*4	0.1	0.5	94	0.688	0.07	89.8	***NM
5	1	0.5	105	0.613	0.07	88.6	1.062

Table 4. Summary of important parameters for homogenous pack experiments.

- Run with pack 2.

** Injected pore volume was not subtracted from recovery.

*** Recovery was not recorded for this experiment.

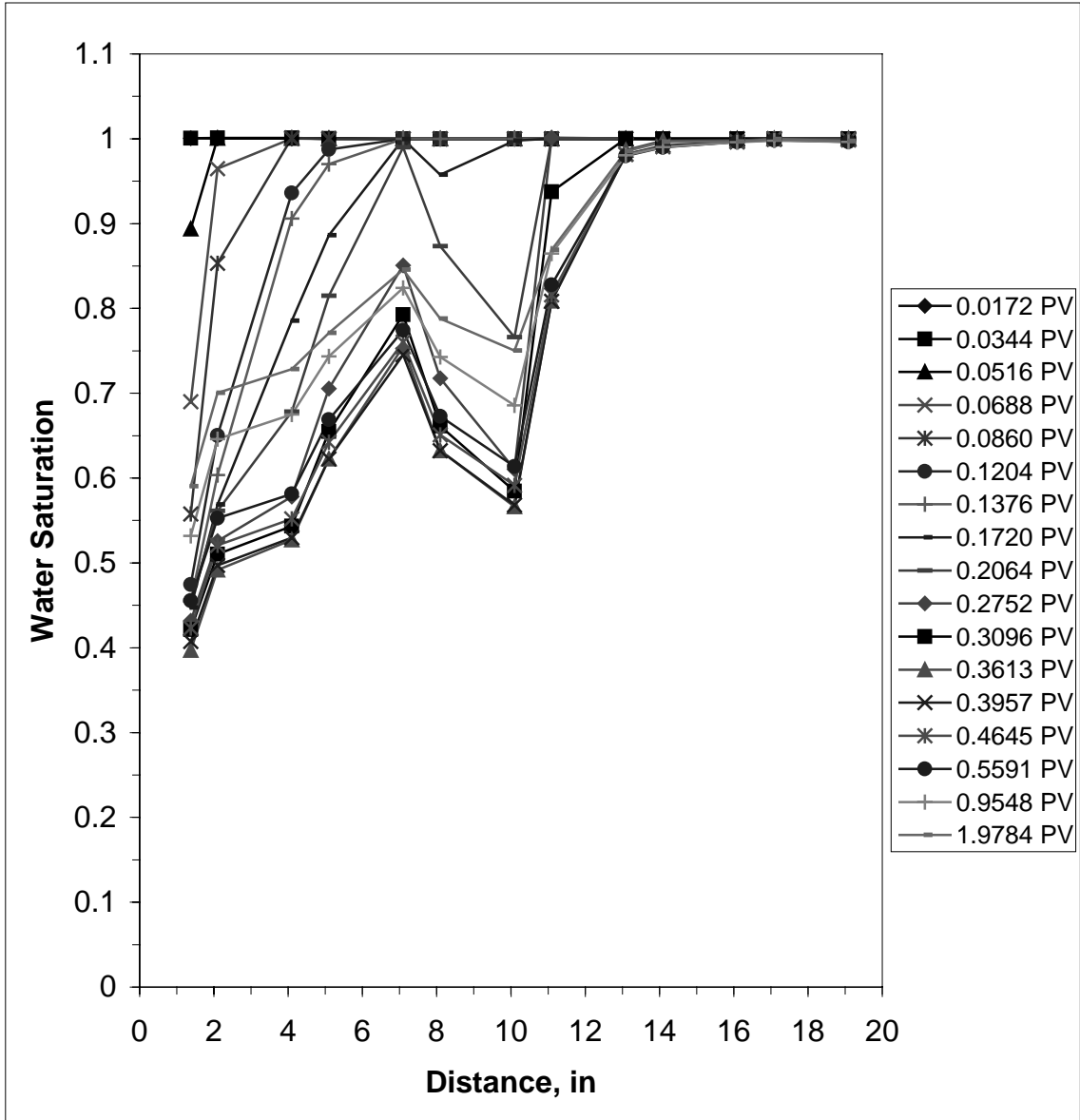


Fig. 6. Water saturation profile for 0.005 wt % foamer solution.

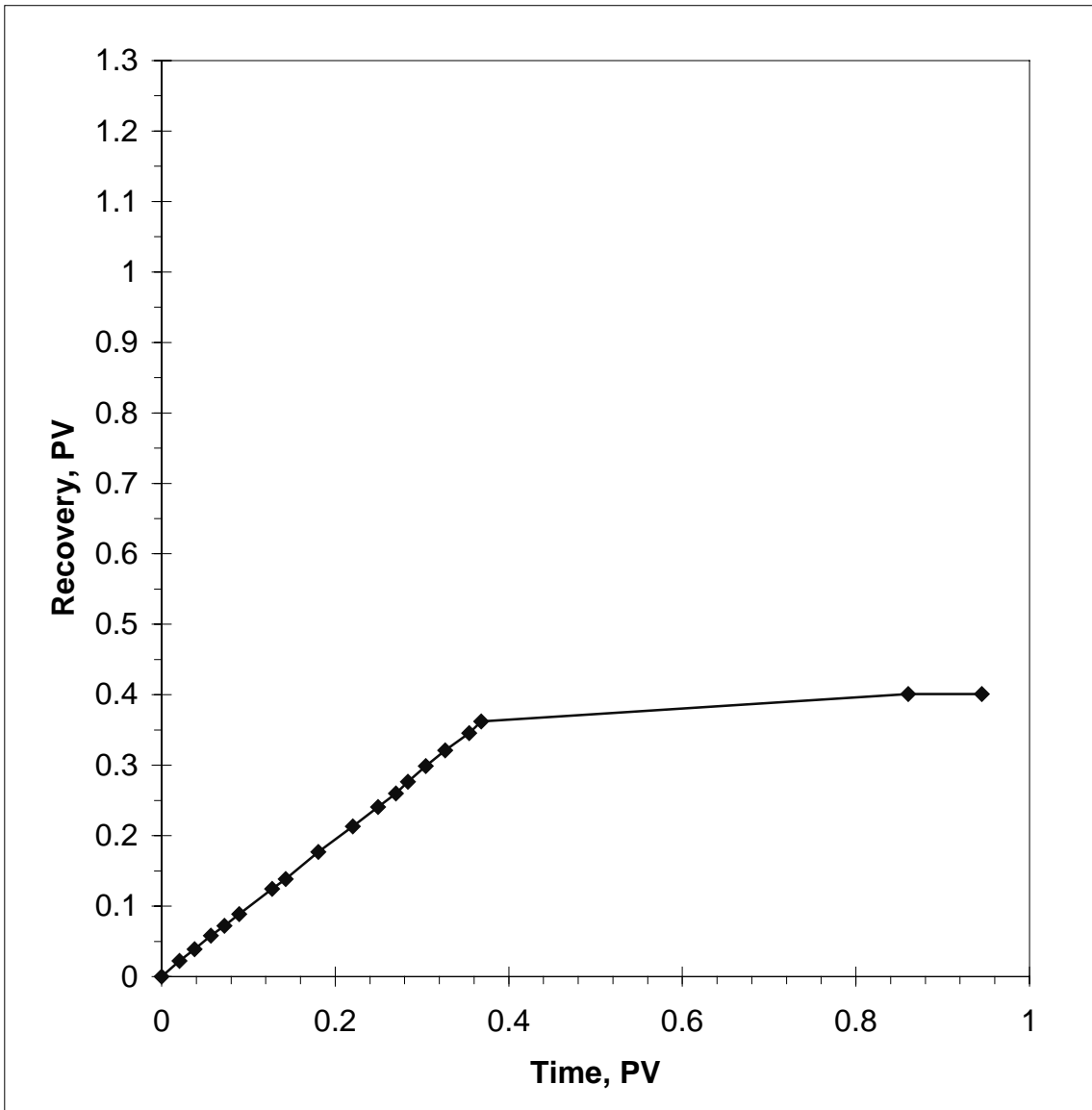


Fig. 7. Cumulative water recovery curve for 0.005 wt % foamer solution.

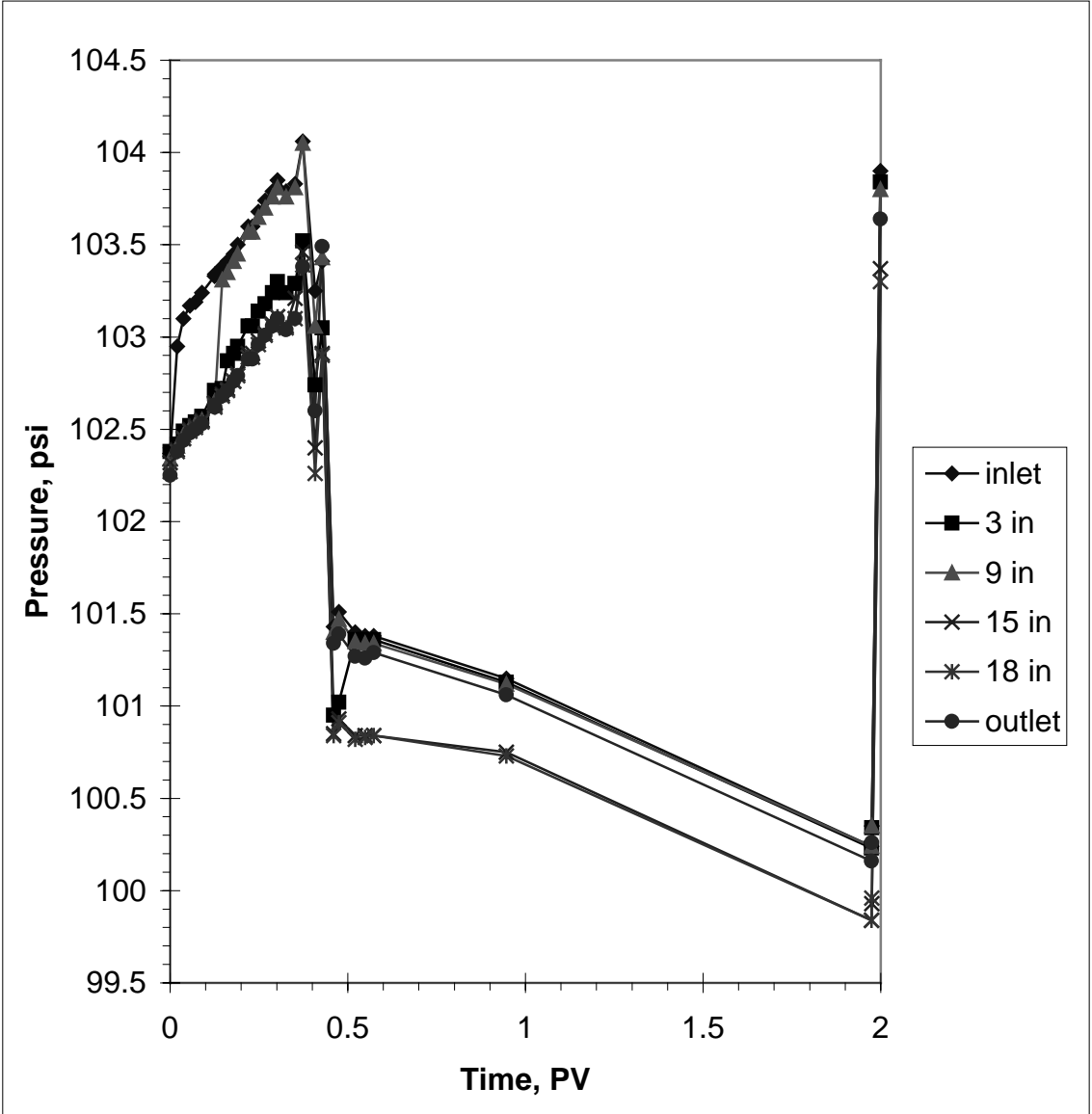


Fig. 8. Measured absolute pressure data along the core for 0.005 wt % foamer solution.

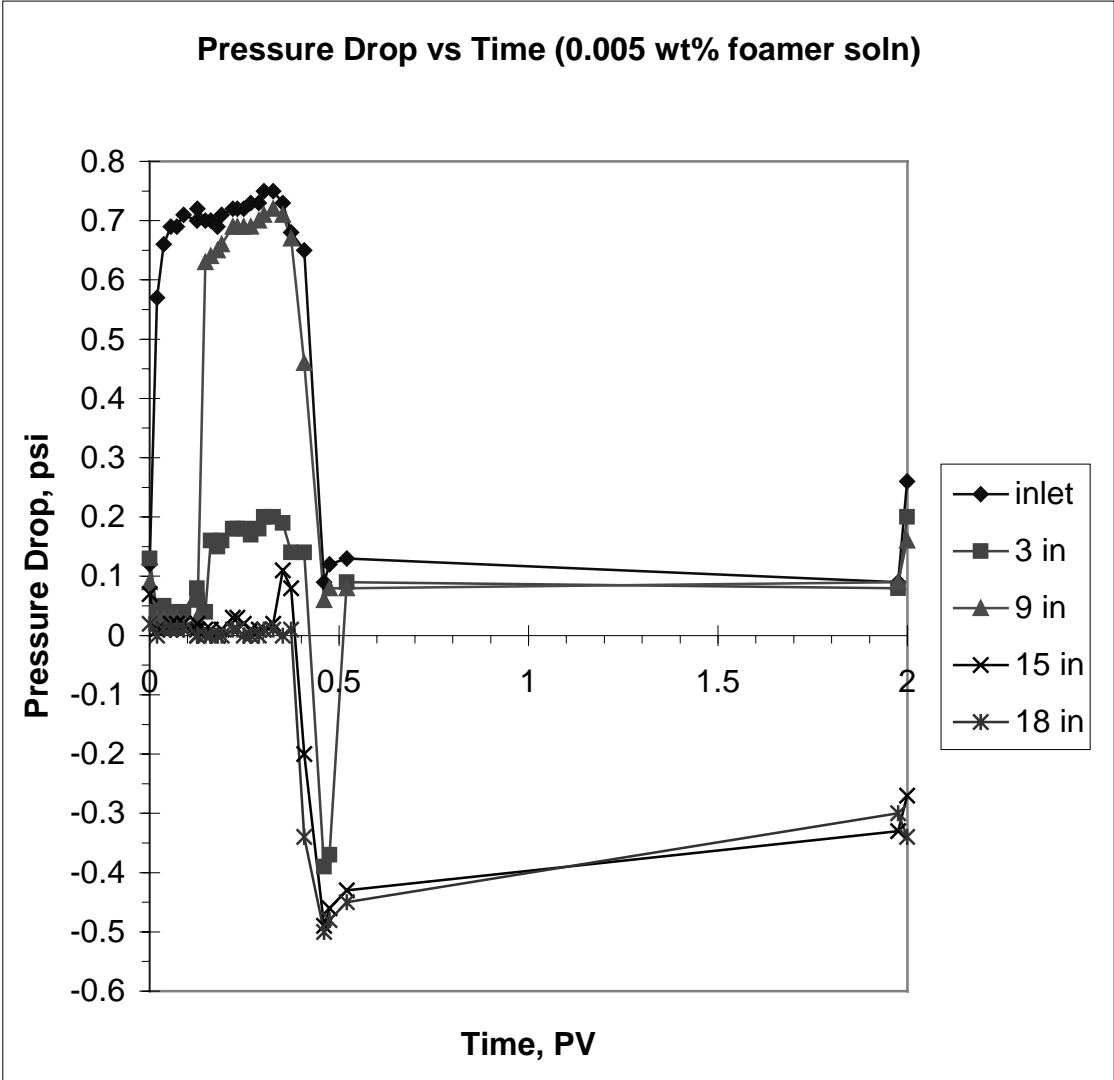


Fig. 9. Pressure drop data along the core for 0.005 wt % foamer solution.

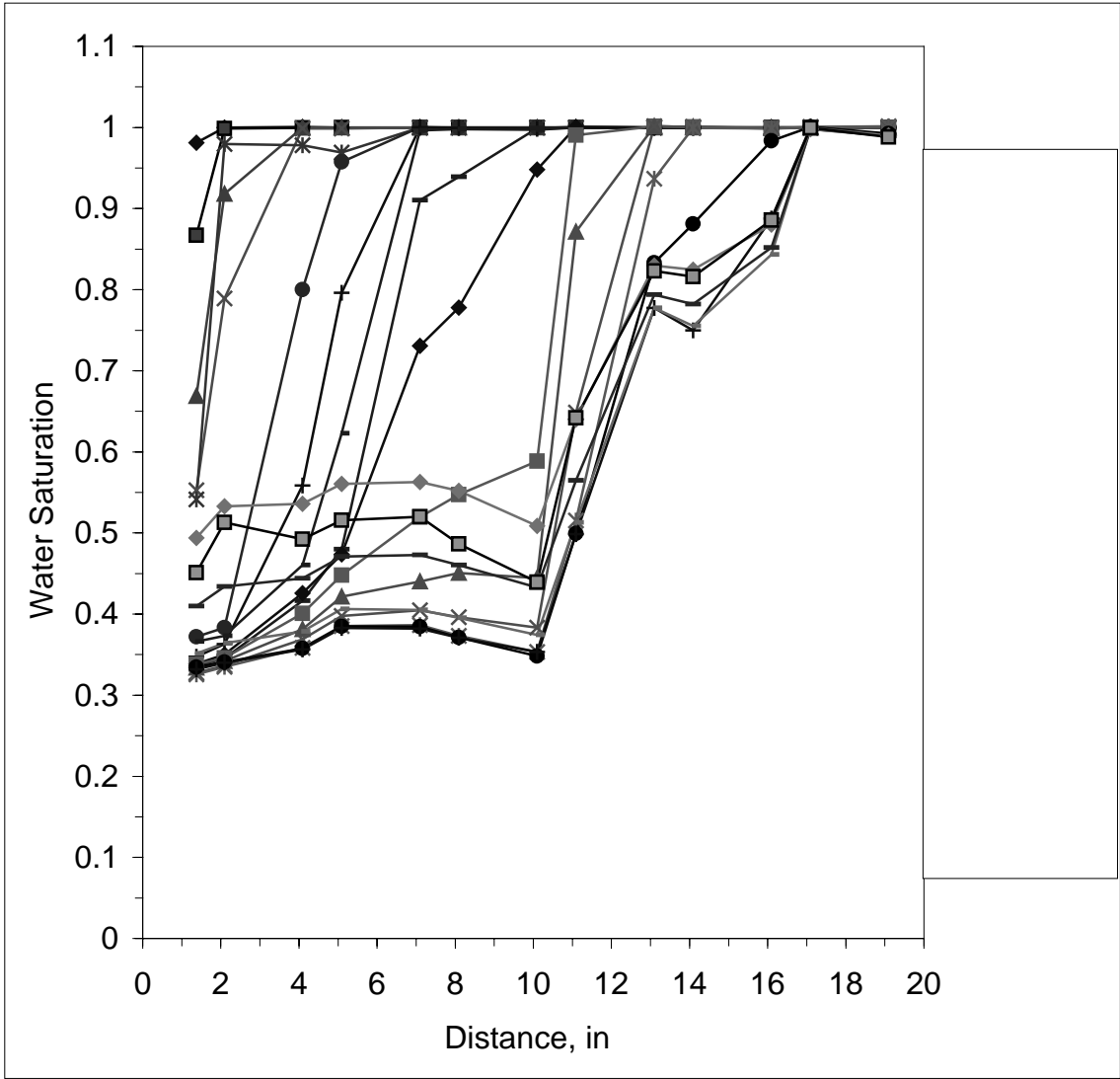
As can be seen in the water saturation curves shown in Fig. 6, sweep efficiency is very low. Water was recovered only in the first half of the core. In this part, recovery is around 50 % and after that no water is recovered. We examined the CT images that were shot in the second half of the core and concluded that we could explain this flow behavior as a capillary end effect. Cumulative recovery at breakthrough was only 0.362 PV. As can be seen in Fig. 7, after one pore volume of injection cumulative water production remains at around 0.4 PV. Almost all the recovery occurs until breakthrough is reached.

After breakthrough, gas follows established flow paths with little resistance and so does not recover any additional water. In Figs. 8-9, we give absolute pressure data measured during the experiment and pressure drop data which is obtained simply by subtracting absolute outlet pressure from the rest of the measured data. The outlet pressure line in Fig. 8 shows us that back-pressure was around 101-102 psi during the experiment. In both pressure plots, breakthrough time is estimated as 0.36 PV. After breakthrough, because we have compressible fluid in the system we observe some experimental errors and also relatively lower pressure values within the core compared to the outlet pressure. But the basic conclusion of these pressure plots is that, there is no significant pressure drop across the core. The maximum pressure drop is 0.72 psi which might be expected in a typical gas injection case without surfactant. These results provide us enough evidence to believe that no foam was generated in the porous medium.

In the next experiment, we prepared a foamer solution with 0.01 wt % surfactant in 0.5 wt % salt. Water saturation profiles, the recovery curve, and pressure profiles for this experiment are given in Figs. 10-13. Again we conducted this experiment in pack 1.

The cumulative injection rate was $0.632 \text{ cm}^3/\text{min}$ (0.45 m/day superficial velocity) at 103 psi back-pressure and gas fractional flow was 88.9% . Liquid rate is $0.07 \text{ cm}^3/\text{min}$.

As can be seen in water saturation curves shown in Fig. 10, sweep efficiency is better compared to the previous case, but still not efficient. Increasing the surfactant concentration showed some positive effects, and 70% of the water in the first half of the core was recovered. But again, because of a capillary end effect almost all of the water in the second half of the core was not displaced. Cumulative recovery at breakthrough has increased significantly to 0.53 PV . After 2.6 pore volumes of injection, cumulative recovery is around 0.6 PV as shown in Fig. 11. As observed in the previous case, water is mostly recovered until breakthrough is reached. If we look at the pressure plots, we see responses similar to those obtained in the $0.005 \text{ wt } \%$ foamer injection case. By looking at the pressure data presented in both Figs. 12 and 13, one can easily estimate the breakthrough time between 0.5 and 0.6 PV . Measured absolute pressure data (Fig. 12) shows that overall system pressure is fluctuating between $103\text{-}105 \text{ psi}$. But no significant pressure difference can be observed between the inlet and the outlet pressure. This is also verified by the pressure drop data. As experienced with the previous foamer solution, the pressure drop across the core is less than 1 psi . So we can conclude that, even though surfactant concentration was increased to $0.01 \text{ wt } \%$ and water recovery has increased significantly, the displacement was still not efficient. In pressure response, no noticeable difference compared to the lower concentration was observed. We generated some weak foam by the help of the porous plate at the inlet, which helped to increase recovery.



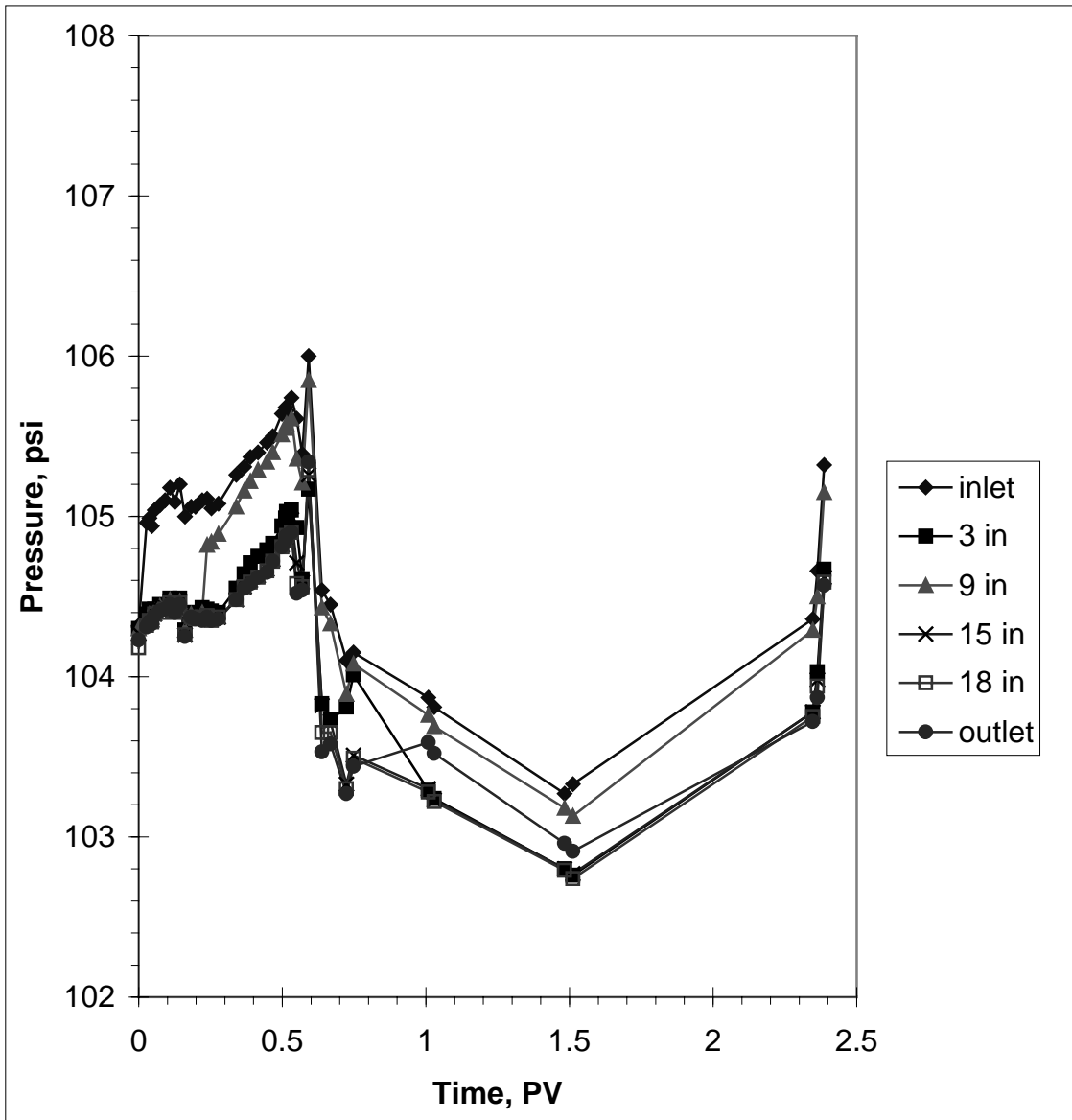


Fig. 12. Measured absolute pressure data along the core for 0.01 wt % foamer solution.

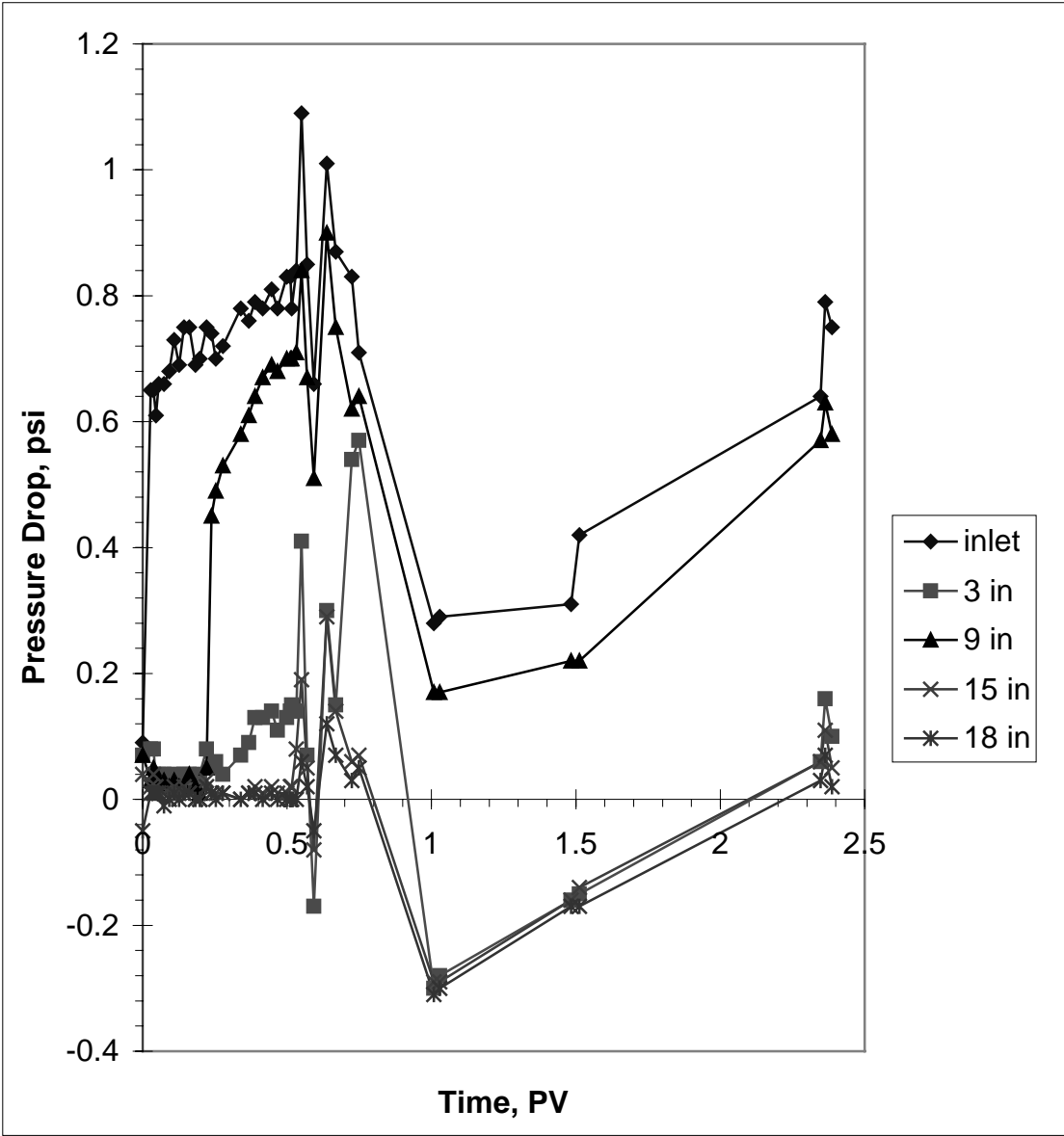


Fig. 13. Pressure drop data along the core for 0.01 wt % foamer solution.

For the next experiment, we doubled the surfactant concentration and increased it to 0.02 wt %. This helps us to understand the transition range between generating weak and strong foam. The total co-injection rate was $0.62 \text{ cm}^3/\text{min}$ (0.44 m/day superficial velocity) at 100 psi back-pressure. The gas fractional flow rate was calculated to be 88.78 %.

The water saturation profile is given by Fig. 14. We did not observe a capillary end effect during this experiment. This led to higher sweep efficiency, and the recovery increased up to 70-80 % all along the core. The cumulative water recovery at breakthrough was measured to be 0.745 PV, which is an indication of stronger foam generation. After 2.4 pore volumes of co-injection cumulative water recovery has reached 0.8 PV (Fig. 15). The back-pressure during the experiment was around 100 psi (Fig. 16). When we look at the pressure drop plot shown in Fig. 17, we see that there is greater pressure drop across the core. As can be seen in the figure, inlet pressure is oscillating between 2-5 psi values. This is likely caused by the porous plate that is placed at the inlet of the core to create permeability contrast and to help foam generation. Foam is generated at the interface between the porous plate and the sand, but because it is still not strong and stable it coalesces when it enters the sand region. This is why the oscillating behavior was observed at the inlet pressure. In sand region, pressure drop response similar to the previous experiments was observed, that is, less than 1 psi. In this experiment, more stable foam was generated, no capillary end effect was observed, sweep efficiency increased to 75 %, and no significant pressure response was recorded.

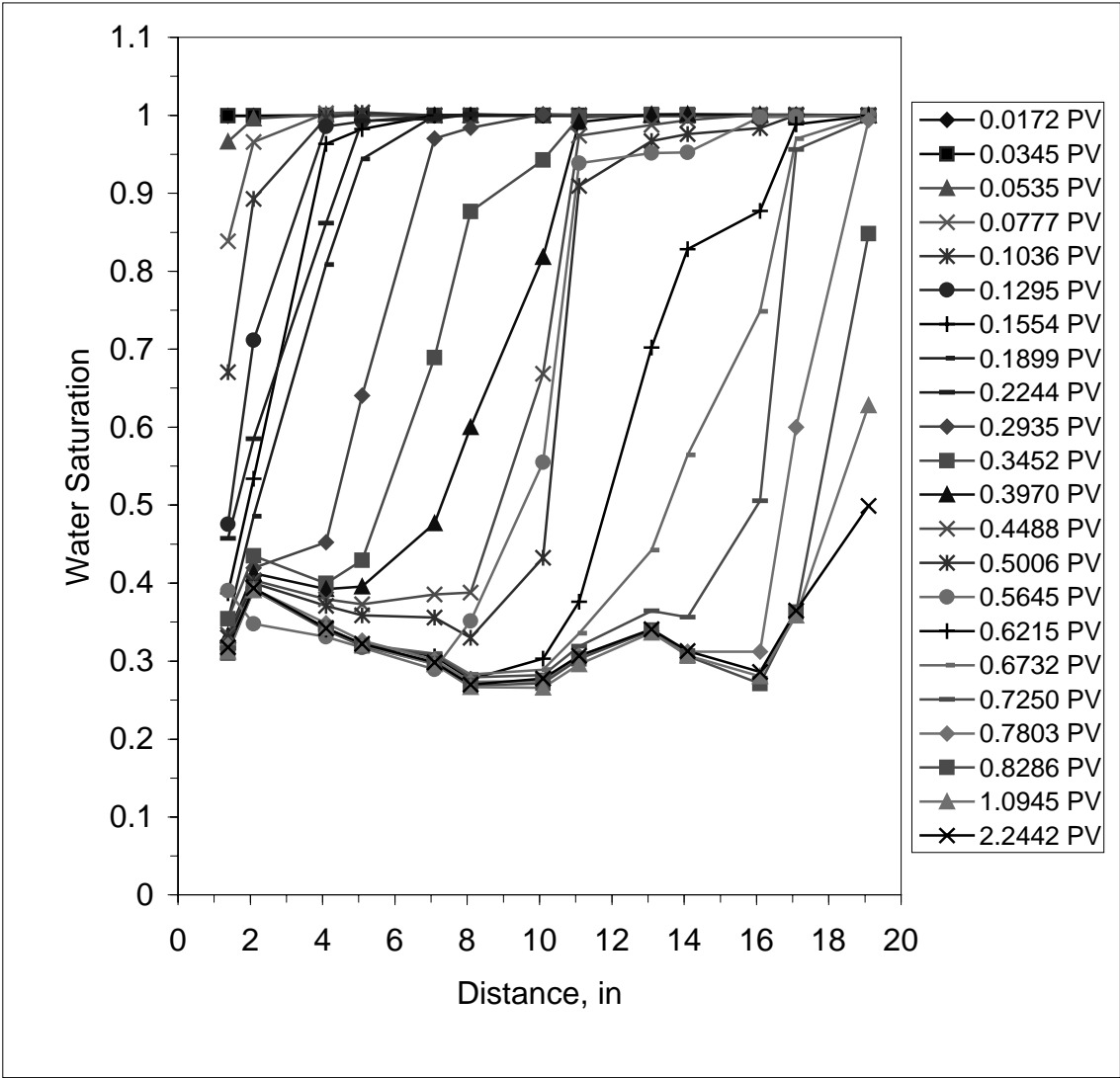


Fig. 14. Water saturation profile for 0.02 wt % foamer solution.

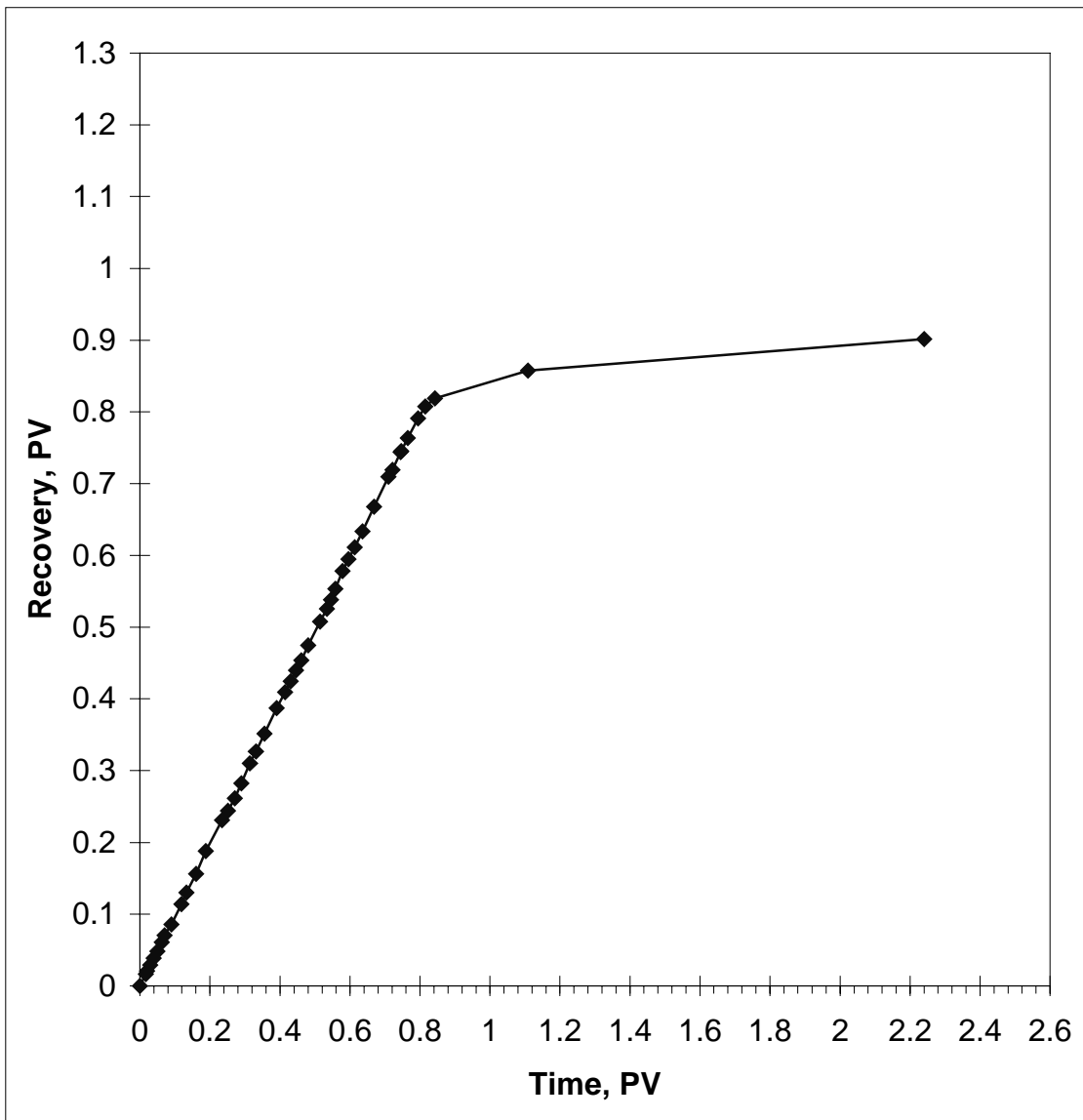
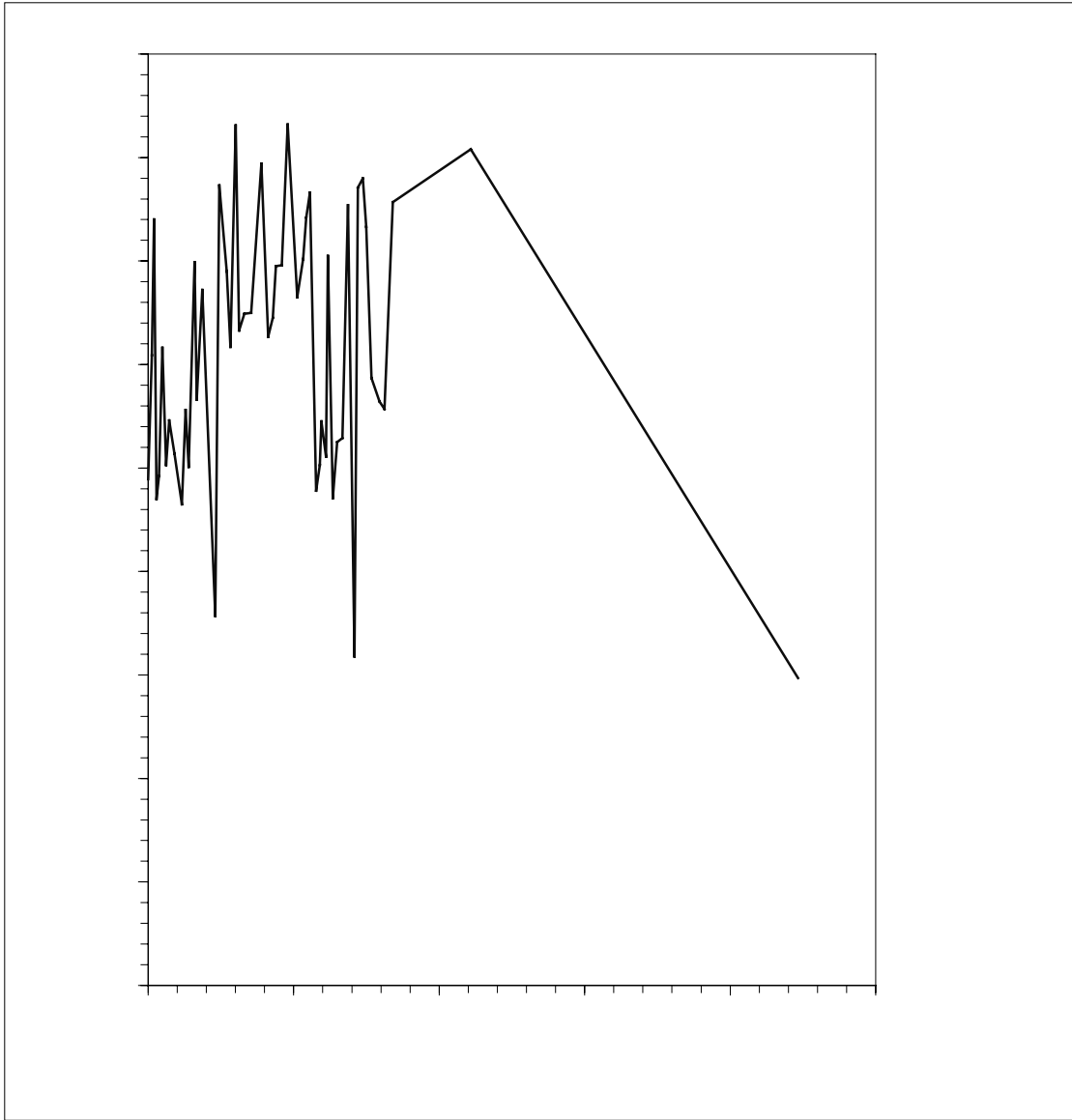


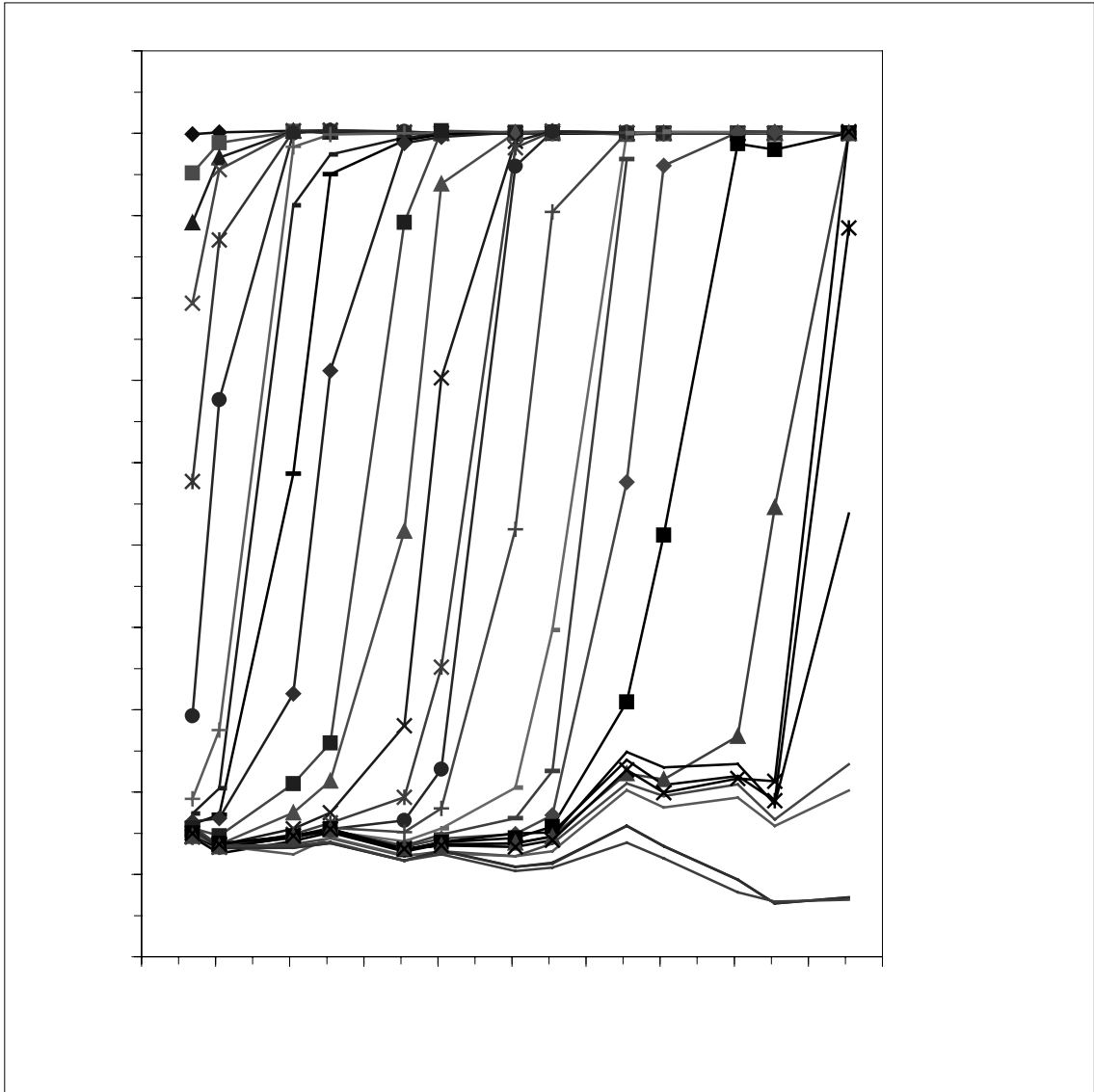
Fig. 15. Cumulative water recovery curve for 0.02 wt % foamer solution.



The next experiment was conducted in pack 2. A 0.1 wt % surfactant and 0.5 wt % salt foamer solution was used. Water recovery was not measured during this experiment. The total co-injection rate at 93 psi back-pressure was 0.688 cm³/min with 89.8 % gas fractional flow. This represents 0.488 m/day superficial velocity.

In this experiment, very effective sweep was observed. As can be seen in Fig. 18, at the end of experiment, almost 90 % of the water in place was recovered, which is significantly higher compared to the previous cases. At the end of one pore volume of co-injection, foam has not broken through yet but the front location is very close to the end of the core. This shows that, most of the recovery occurred before breakthrough. Saturation profiles show an almost piston-like displacement.

Besides sweep efficiency, drastic changes in the pressure responses were observed. Back-pressure was around 93 psi during the experiment (Fig 19). Pressure-drop data was significant with respect to distance for different times. This is different from the previous experiments. For the first time, noticeable pressure drop was measured across the core. As can be seen in Fig. 20, at the end of one pore volume of co-injection 6.5 psi pressure drop across the core was measured. Interestingly, pressure drop continued increasing after breakthrough, and when steady state was reached a 25 psi pressure drop was recorded across the core. These results provide evidence that strong and stable foam was generated in the sand pack. This stable foam lead to very good sweep efficiency where almost all the mobile water was recovered, and increased the flow resistance in the system such that high pressure drop values resulted. No negative



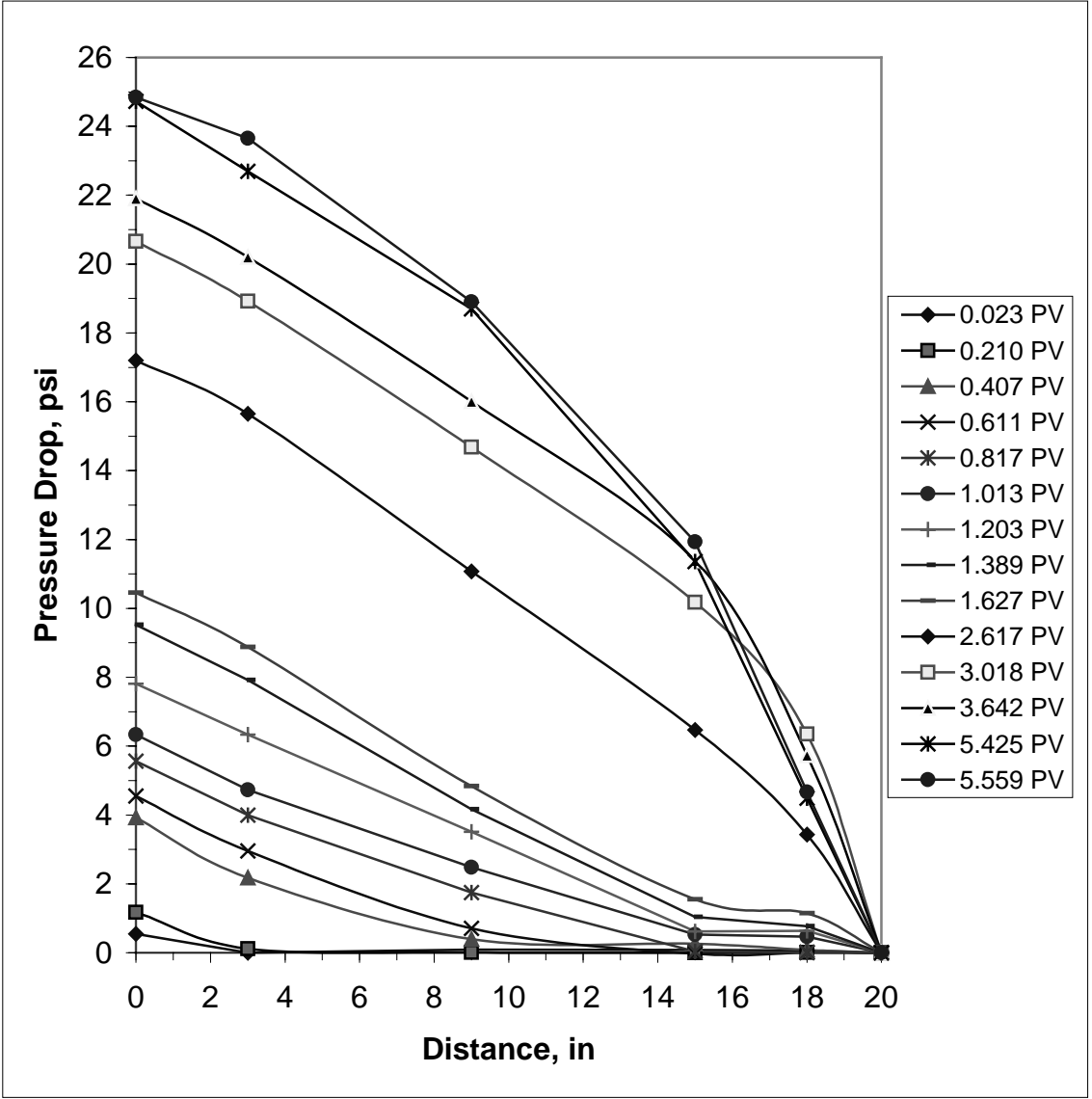


Fig. 20. Pressure drop data along the core for 0.1 wt % foamer solution.

pressure drop values were recorded, possibly because of the presence of stable foam. Because pressure responses are very stable, it is not possible to estimate accurately breakthrough time by using pressure data in Fig. 19. After 2.6 PV of injection it is observed that there is higher pressure drop towards the end of the core (Fig. 20). This means there is more flow resistance, hence more finely textured, stable foam in that region.

The final experiment was conducted with 1 wt % surfactant solution in brine (0.5 wt % salt) in pack 1. The cumulative injection rate was $0.61 \text{ cm}^3/\text{min}$ which corresponds to 0.435 m/day superficial velocity at 105 psi back-pressure. Gas fractional flow rate was 88.6 %. The liquid rate was $0.07 \text{ cm}^3/\text{min}$.

Water saturation profiles for this experiment are given by Fig.21. As observed in the previous case, sweep efficiency is very high. Saturation curves are sharper and a more piston-like displacement is observed. As observed in the 0.1 wt % case, at 1 PV of injection, the foam front is about to breakthrough which is an indication of very effective sweep. Almost all the movable water was recovered when breakthrough was reached. At the breakthrough, the cumulative water recovery was measured to be 1.062 PV (Fig. 22). Note that, some liquid was injected into the core and this resulted in a greater than 1 PV recovery.

Pressure profiles are very similar to the 0.1 wt % foam experiment except for the magnitude. Pressure drop increased significantly compared to the previous case. This implies stronger and more stable foam bubbles were generated leading to more flow

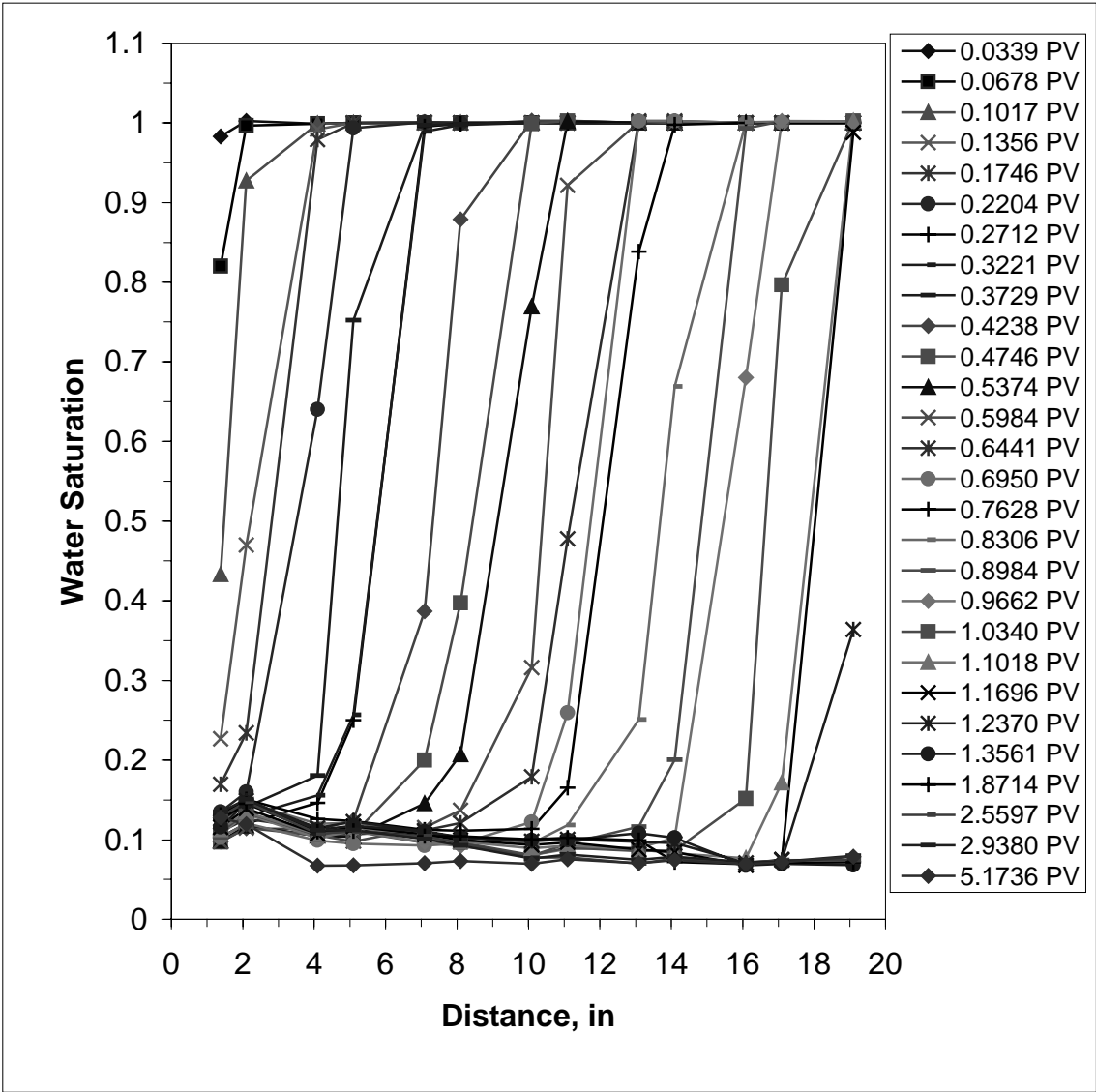


Fig. 21. Water saturation profile for 1.0 wt % foamer solution.

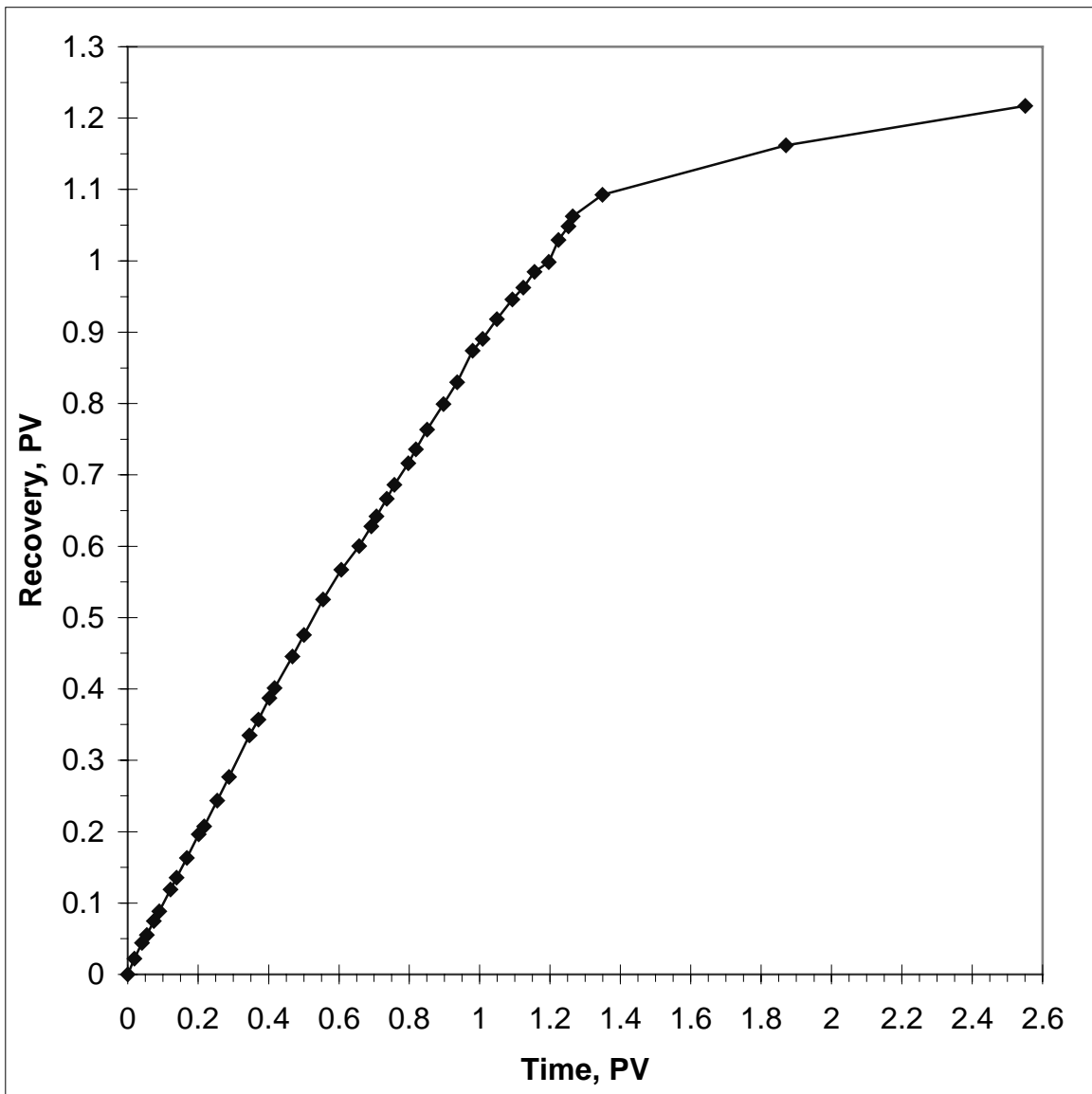
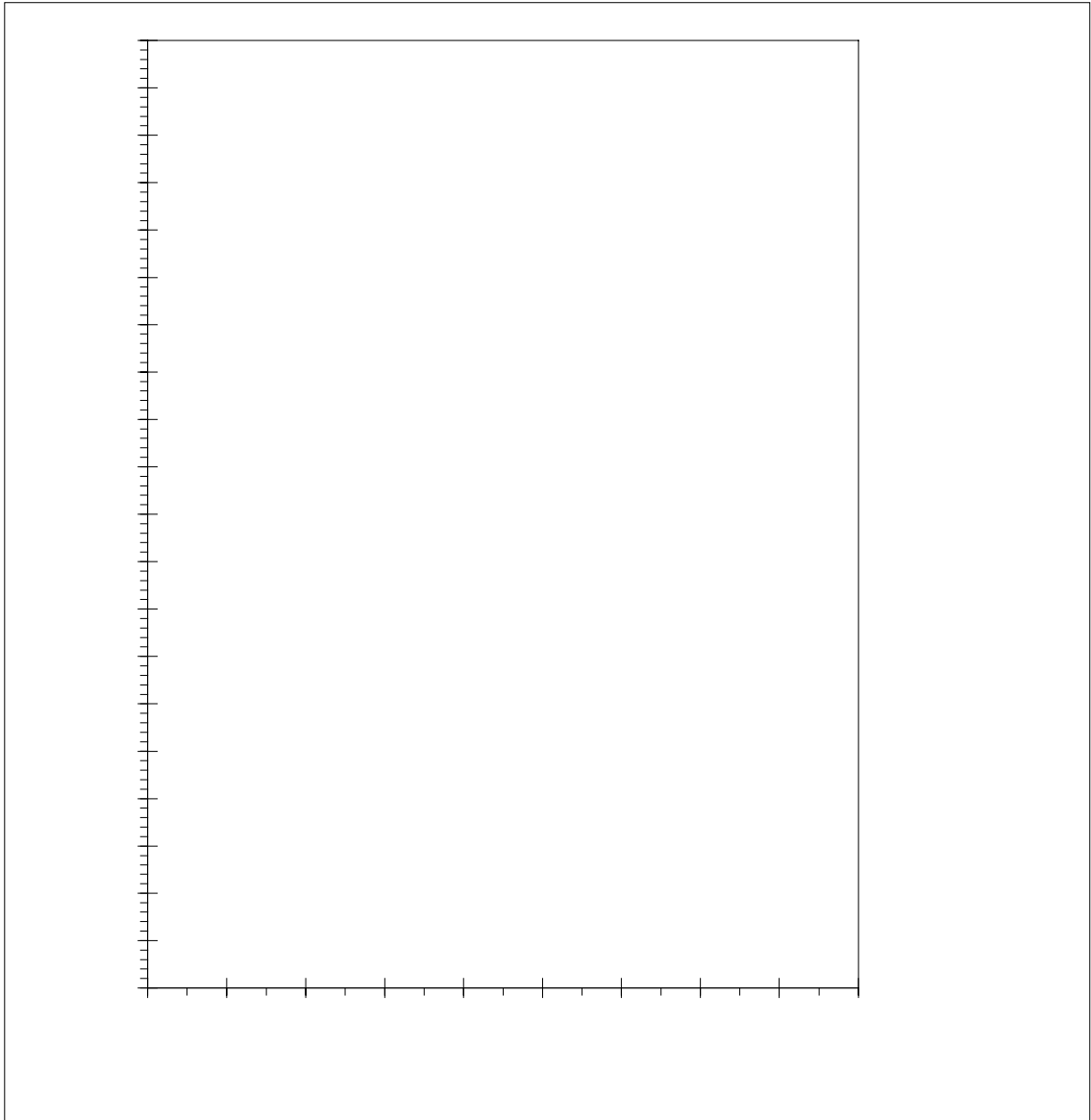


Fig. 22. Cumulative water recovery curve for 1.0 wt % foamer solution.



resistance in the porous media (Figs. 23-24). Back-pressure was around 105 psi (Fig. 23). At the end of one pore volume of co-injection a 22 psi pressure drop was recorded across the core which is almost 3.5 times greater than the 0.1 wt % case. Pressure drop continued increasing after breakthrough and when steady state was reached, an 87 psi pressure drop was measured. In this final experiment, recovery has increased, almost all mobile water was recovered prior to breakthrough, and significant pressure drop values were recorded. As observed in the previous experiment, the slope of the pressure drop lines increase towards the end of the core (Fig. 24). More finely textured foam bubbles start forming at the end of the core and when steady state is reached almost a straight pressure drop line is observed, which means the core is filled with finely textured foam bubbles.

If we summarize, foam flow experiments were conducted in two homogenous sand packs to investigate the effect of surfactant concentration on foam flow in porous media. Experiments were started with very low concentration (0.005 wt %) and increased gradually up to 1 wt %. It was observed that, in the first experiment no foam was generated, and as a result water recovery was very low. Also, no pressure drop was measured. At 0.01 wt % surfactant concentration, very weak foam was generated and this lead to a recovery increase, but still no significant pressure drop was observed. When the surfactant concentration doubled to 0.02 wt %, good sweep efficiency was achieved all along the core. This was significantly different compared to the previous case, and we began to see a pressure drop response to foam. Thus we claim that, stable foam generation began at this surfactant concentration. In the higher concentrations such as 0.1 and 1 wt %, almost all mobile water was swept out of the sand pack by foam, and large

pressure drop values were obtained. This was evidence of strong and stable foam generation. In all the experiments, significant water recovery occurred until water breakthrough was reached and after that a very little amount water was recovered.

HETEREGENOUS PACK EXPERIMENTS

Previous studies of foam generation and transport were conducted, mainly, in one-dimensional and homogeneous porous media. However, the field situation is primarily heterogeneous and multidimensional. To begin to bridge this gap, we have studied foam formation and propagation in an annularly heterogeneous porous medium. The experimental system was constructed by centering a cylindrical Fontainebleau sandstone core inside an acrylic tube and packing clean Ottawa sand in the annular region. In this way, an order of two magnitudes of permeability contrast was created. Experiments with and without crossflow between the two porous media were conducted. The aqueous phase saturation distribution is garnered using X-ray computed tomography. In the next two sections, we detail experimental setup and procedures, and then discuss the results.

4.1.

Experimental Setup and Procedures

The centerpiece of the experimental program is a heterogeneous porous medium. It is constructed by centering a 0.050 m diameter and 0.368 m long Fontainebleau sandstone core inside a long, cylindrical, acrylic core holder. The inner diameter of the acrylic tube is 0.089 m and total length is 0.65 m. The annular space between the sandstone and the coreholder wall is packed with Ottawa sand. Similarly, the remaining 0.282 m of coreholder is packed with sand. Hence, the tube contains a heterogeneous portion consisting of sandstone and sand, and a homogeneous portion filled with sand. For experiments where we seek to prevent exchange of fluid between the sandstone and the sand, a heat-shrink Teflon tube is fit around the sandstone. In this case, only the circular faces at the beginning and end of the Fontainebleau core are left open to flow. When cross-flow is not prevented, we make no special preparation of the sandstone core.

Figure 25 is a reconstructed image of the porosity field measured using the CT scanner. Further details on the scanner and imaging methods will be given later, but the sandstone and sand portions of the porous medium are labeled and apparent in Fig. 25. Average porosity values obtained with CT along both the sand and sandstone portions of the core are displayed in Fig. 26. Each component of the heterogeneous porous medium is relatively homogeneous with an average sandstone porosity of 0.14 and an average sand porosity of 0.32. The Ottawa sand permeability was measured at $6.7 \mu\text{m}^2$ and the Fontainebleau sandstone permeability is $0.1 \mu\text{m}^2$. Both values are permeability to brine. The contrast in permeability between the sand and sandstone is 67 to 1.

the heterogeneous end, foam generation in an initially liquid-filled heterogeneous porous medium can be observed. Unfortunately, coreholder design precluded the installation of pressure taps to measure the in-situ pressure profile.

Nitrogen (N_2) is injected into the porous medium saturated with foamer solution at a rate of 3 sccm (standard cubic centimeters per minute) using a Matheson (Montgomeryville, PA) Model 8240 0-10 sccm mass flow controller. Nominally, the superficial gas velocity is 0.67 m/day relative to the outlet pressure of 101325 PA. Foamer solution was not injected simultaneously with the gas because such experiments in one-dimensional, homogeneous sand packs can lead to high pressure drops as shown in the previous chapter, and we did not wish to over-pressurize the experimental system. Previous one-dimensional experiments using gas only injection and a similar surfactant and sand resulted in moderate pressure drops (Fergui *at al*, 1995).

Through the combination of communicating and noncommunicating heterogeneities and injection into homogeneous or heterogeneous portions of the core, four different experiments are possible:

1. Injection across the heterogeneous side, noncommunicating sand and sandstone
2. Injection across the heterogeneous side, communicating sand and sandstone
3. Injection across the homogenous sand, noncommunicating sand and sandstone
4. Injection across the homogenous sand, communicating sand and sandstone

Figure 27 shows schematically each of these cases and indicates where gas is injected. A dark, solid line indicates the heat-shrink jacket if present.

The surfactant is an alpha olefin sulfonate (AOS C14-C16), which was also used in the homogenous pack experiments. A concentration of 0.1% by weight active surfactant in a 0.5 wt % salt brine was chosen as the optimal foamer solution. As explained in Chapter 2, for the 0.5 wt % brine, strong foaming action, as witnessed by pressure drop, is found once the CMC is exceeded. Further, no benefit is found when surfactant concentration is increased above 0.1 wt % in either the pressure-drop or surface-tension data. Hence, this 0.1 wt % surfactant concentration was chosen (Fig. 2).

An experiment begins by flushing the porous medium with gas (CO_2 or N_2) until it is free of liquid. A dry scan is made. If needed, the core is refilled with CO_2 , and saturated with brine to 100% water saturation, because the CO_2 is soluble in the brine. At the minimum, 10 pore volumes of surfactant solution are injected to saturate the solid and aqueous phases with surfactant. A wet scan of the porous medium is then obtained. Once the porosity field has been determined, CT is used to confirm that 100 % liquid saturation is obtained. If it has not, more foamer solution is injected to dissolve the CO_2 . Once an S_w of 100% is obtained, N_2 is injected at a constant rate. The progress of foam generation is seen directly in the CT data collected. Gas is injected until foam breakthrough at the outlet occurs and is continued for an additional 0.5 to 1. PV.

Porosity and aqueous-phase saturation fields are measured on 18 volume sections equally distributed along the core using a fourth generation (1200 fixed detectors)

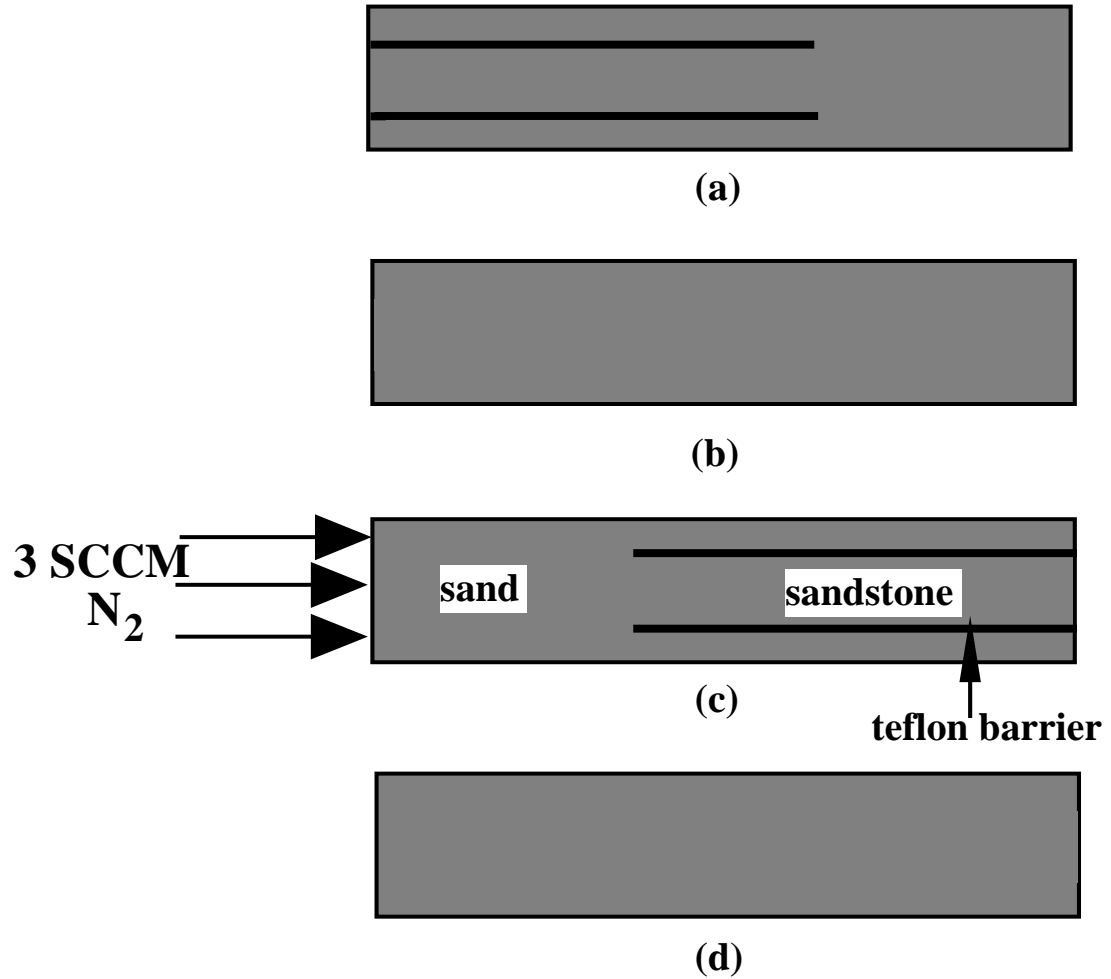
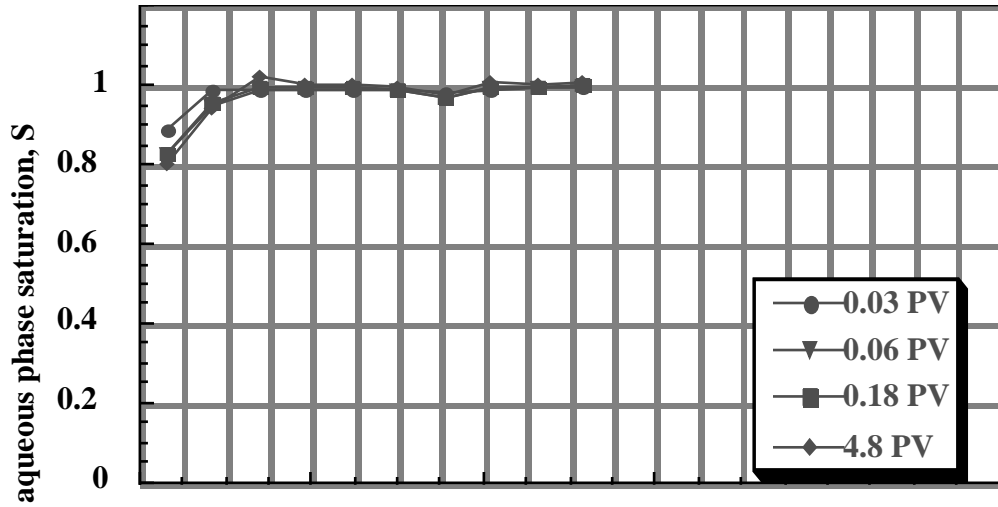


Fig. 27. Configuration of heterogeneous porous medium during experiments. Gas is injected at the left face.

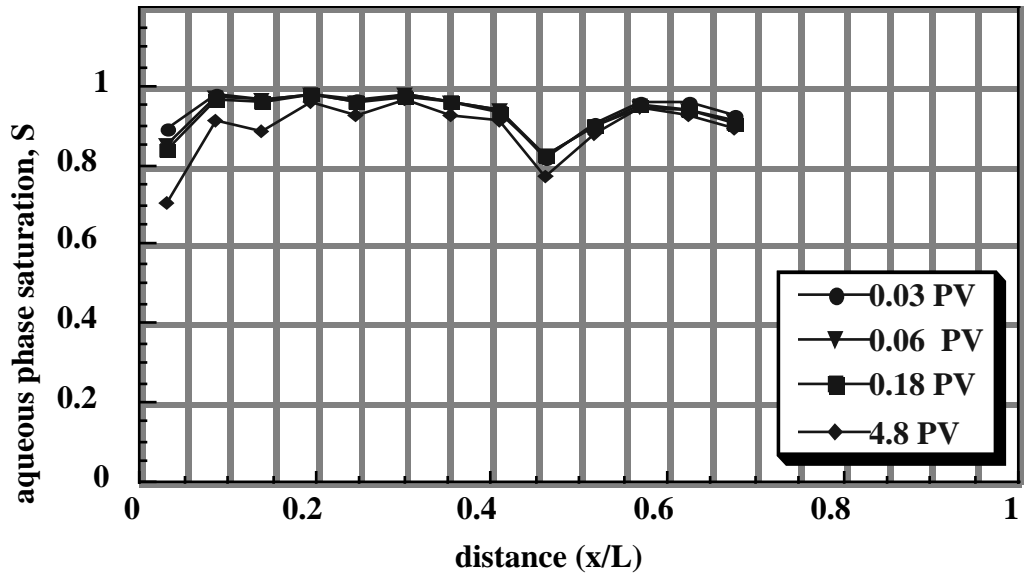
Picker™ 1200 SX X-ray scanner. Typically, the voxel dimension is (0.25mm by 0.25mm by 4mm). The acquisition time of one image is 7 seconds while the processing time is around 40 seconds. The total time of measurement is short enough to capture accurately the position of the front and construct saturation profiles along the core.

3.2 Results and Discussion

To provide a baseline, gas was injected at 3 sccm into surfactant-free cores. Figure 28 illustrates gas flow in the absence of foam when heterogeneities communicate. Saturation values are obtained by averaging the saturation for each voxel in a cross section for the sandstone and sand regions, respectively. Time is reported nondimensionally in pore volumes of injected gas and distance is measured from the inlet. Figure 28a shows the saturation profiles for the sandstone, while Fig. 28b the profiles for the sand. Straight lines connect the individual data points. Gas displacement of water is poor. Strong displacement fronts are not witnessed and even after 4 PV of gas injection, water saturation remains high. In this case, gas breakthrough occurs at 0.05 PV and the total production at 4.5 PV is about 0.1 PV. In the case of noncommunicating heterogeneities, gas breakthrough occurs at 0.11 PV and total water production at 3 PV is only 0.17 PV. As can be seen in Fig. 29, more water is recovered from the sandstone region. This is because the endcap does not distribute the injected gas properly. Most of the injected gas goes into the sandstone, which is in the center near the gas inlet fitting. Because there is a teflon jacket around the sandstone, gas can not redistributed and mostly progresses in this low permeability region.

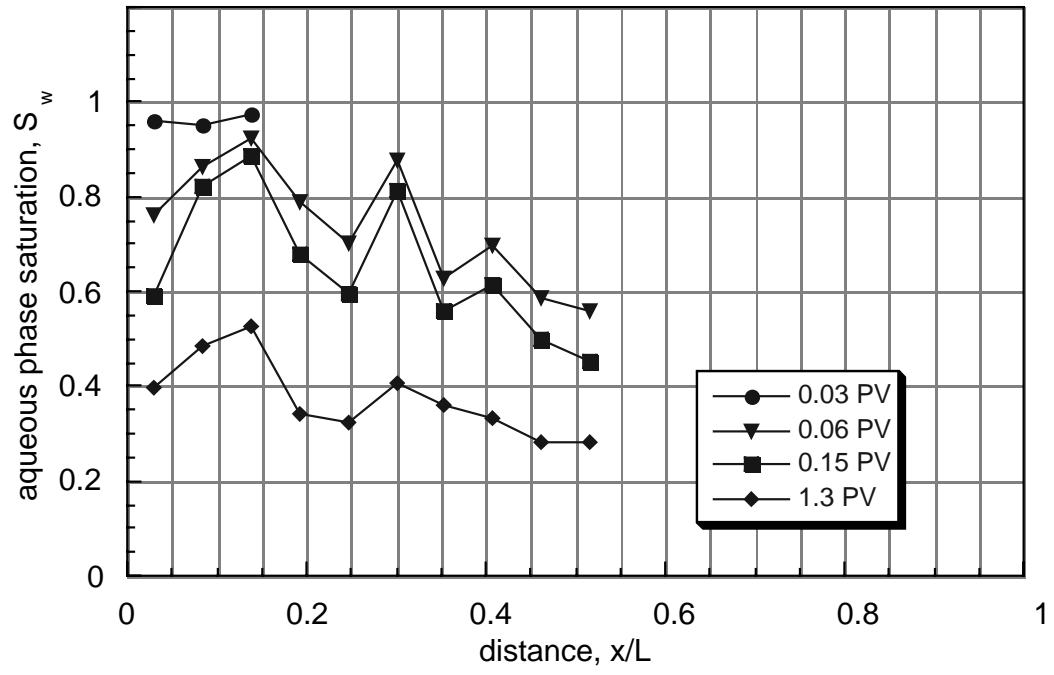


(a)

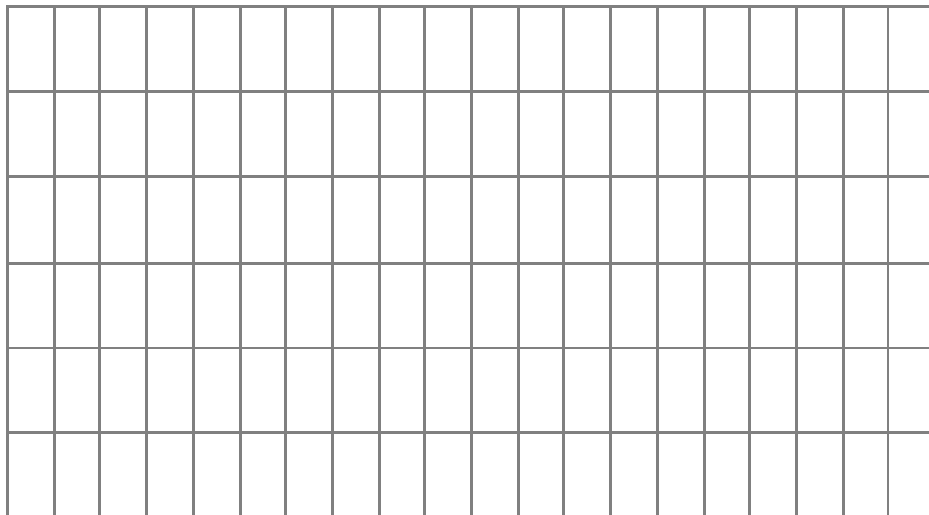


(b)

Fig. 28. Transient aqueous phase saturation profiles for gas-only displacement with crossflow: (a) sandstone and (b) sand regions. Heterogeneous side injection.



(a)



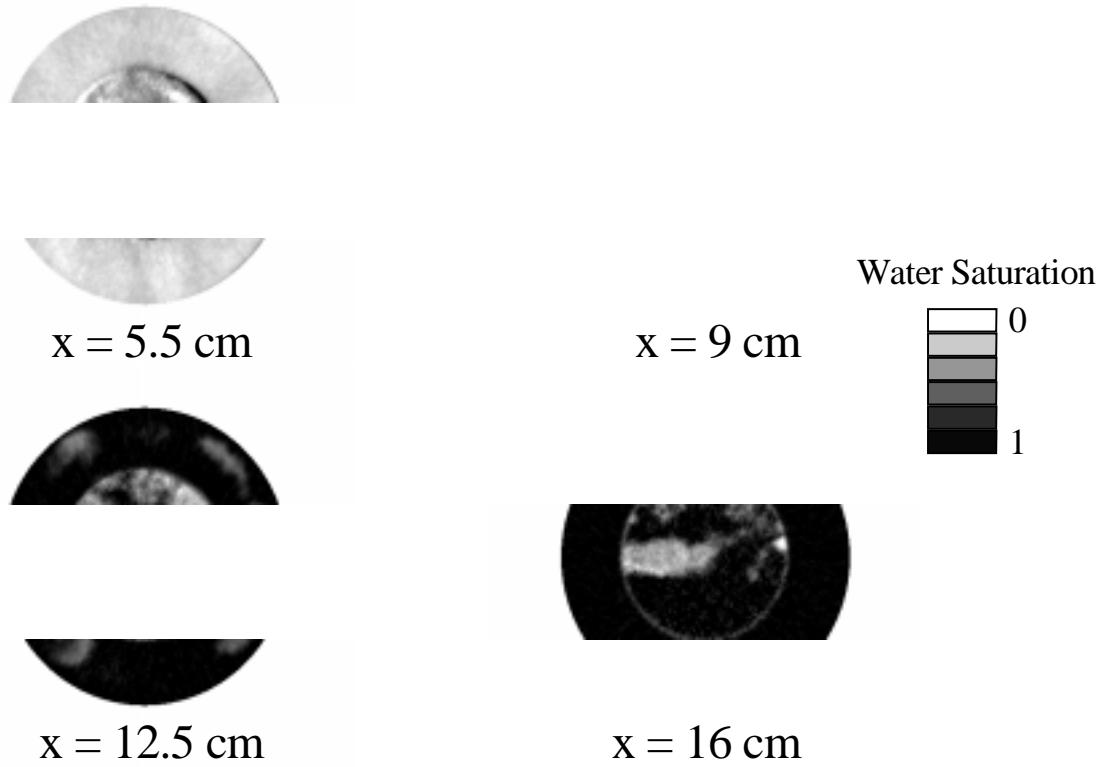
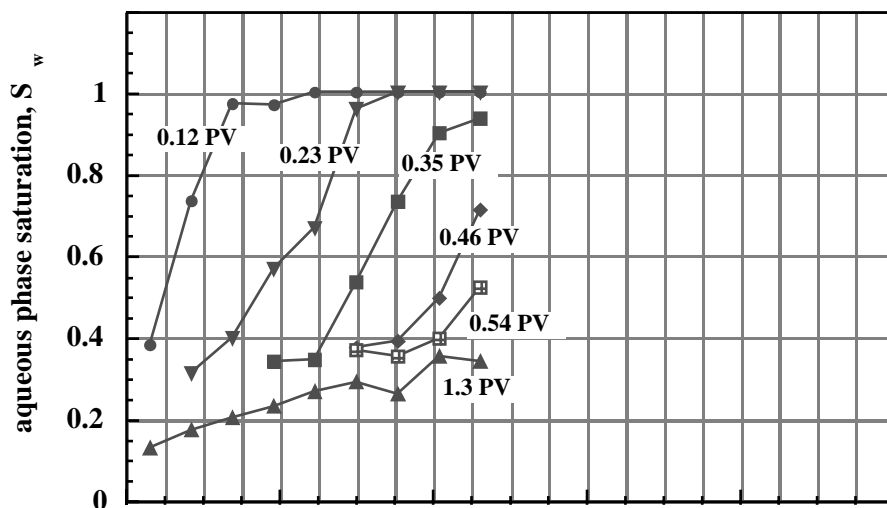
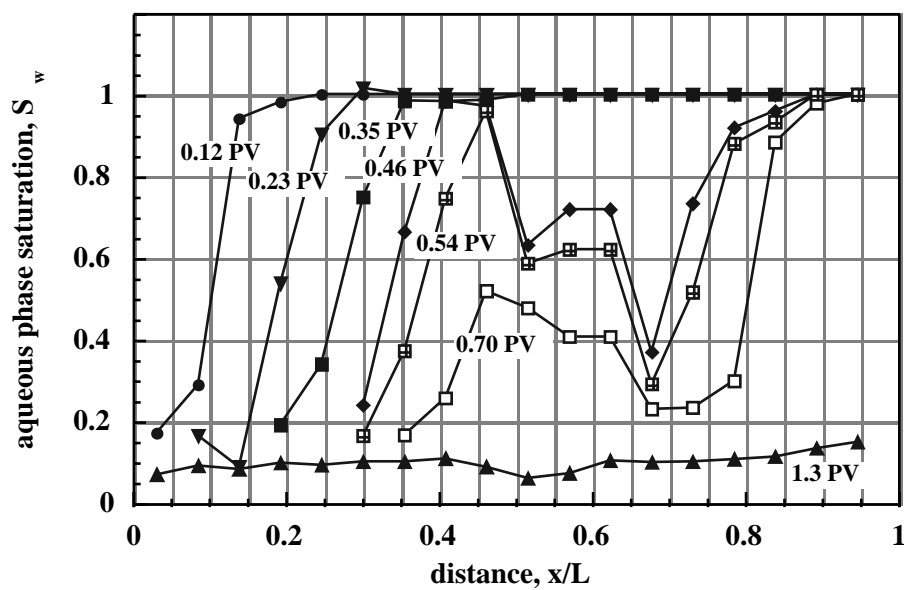


Fig. 30. Water saturation profiles in the heterogeneous core section, $t = 0.23$ PV. Cross flow is not permitted. Heterogeneous side injection



(a)



(b)

Fig. 31. Transient aqueous phase saturation profiles for displacement without crossflow: (a) sandstone and (b) sand regions. Heterogeneous side injection.

The first point to note is that desaturation of both the sand and sandstone by foamed gas is efficient. Saturation fronts are relatively steep and sharp in both porous media. The entire porous medium is saturated with foamer solution initially and S_w downstream of the front is everywhere 1. In the case of the sandstone, S_w immediately following the passage of the foam front is about 0.3 whereas in the sand it is roughly 0.15. That is, following desaturation by foam, each layer is within a few saturation units of its irreducible saturation. Foam has effectively diverted a portion of the injected gas into the sandstone.

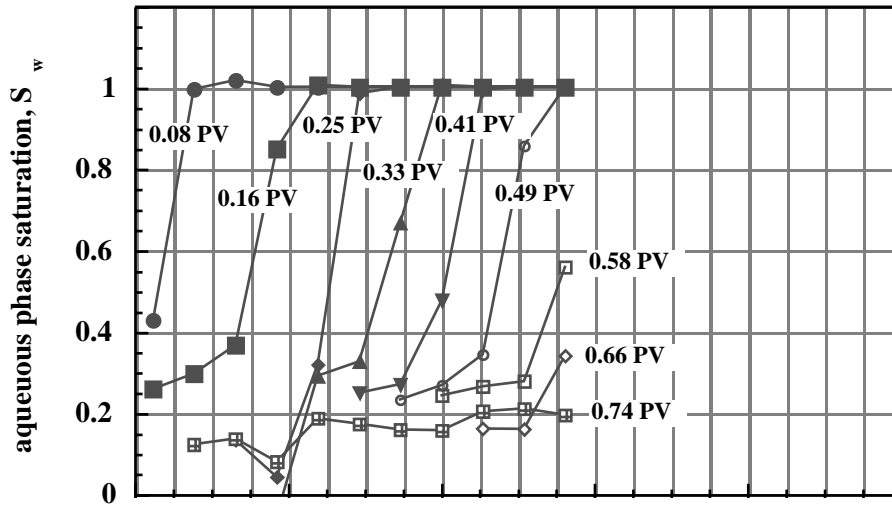
Secondly, the position of the saturation fronts as a function of time tells an interesting story. When t equals 0.12 PV the leading edge of the foam front in both the high and low permeability media is at a dimensionless position of 0.14. At the succeeding time of 0.23 PV the front in the sandstone is at x/L equal to 0.3, while in the sand it is slightly behind at x/L equal to 0.26. At a t of 0.35 PV, it appears that the foam front has just exited the sandstone. The leading edge of the foam front in the sand at this same time significantly lags behind at a position of 0.35. Examination of the saturation profiles at 0.46 PV confirms this trend. The saturation at x/L equal to 0.45 in the sandstone clearly shows that foam has pushed its way through the sandstone core and exited into the sand. On the other hand, the foam front pushing through the annular sand region is only positioned at x/L equal to 0.4. It is apparent that the foam front in the low permeability layer moves more quickly than in the high permeability layer. This fact is also evidenced in the raw saturation data in Fig. 30. In the discussion, we will rationalize this behavior in terms of the effect of capillary pressure on foam texture.

At times of 0.46, 0.54, and 0.70 PV the effect of the foam fronts moving at different speeds in each media can still be seen in the saturation profiles. The foamed gas exiting the sandstone results in fronts positioned in the neighborhood of x/L from roughly 0.75 to 0.85. A second trailing front is also apparent. For instance, at 0.70 PV this trailing front is positioned at roughly 0.45. This second front results from the foamed gas and water exiting the annular region packed with sand as well as water that was not displaced in the completely sand-filled region by the first foam front. By 1.3 PV, the average aqueous-phase saturation in the sand is about 0.10 and desaturation is complete.

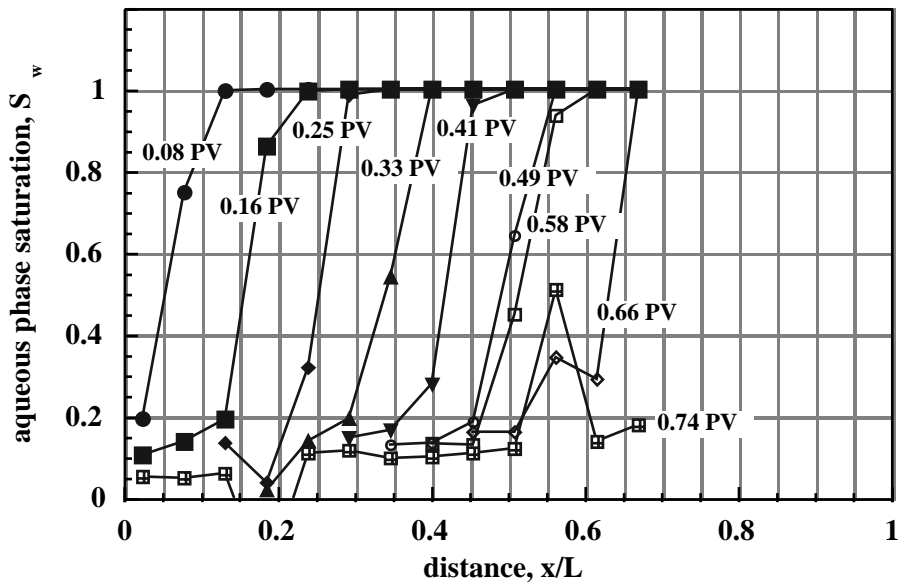
Communicating layers, heterogeneous face injection. The configuration is similar to the first case, except that the heat-shrink Teflon is absent from the sandstone. The sandstone and the sand are thereby in capillary communication and free to exchange fluid along the length of the sandstone.

Figure 32 presents the results of the displacement in a fashion similar to that in Fig. 31. Sandstone saturation profiles are given in Fig. 32a and sand profiles in Fig. 32b. Again, strong and steep displacement fronts in both the sandstone and sand are witnessed. Foam effectively desaturates each layer. In contrast to Fig. 31, the displacement fronts in each porous medium move at the same rate. At times of 0.25, 0.33, and 0.41 PV front position is 0.3, 0.4, and 0.45, respectively. At the shortest time of 0.08 PV, displacement fronts do not coincide exactly. This is likely an inlet artifact.

Displacement fronts that move with identical velocity in communicating heterogeneous zones is also the expected result for the propagation of unfoamed gas



(a)



(b)

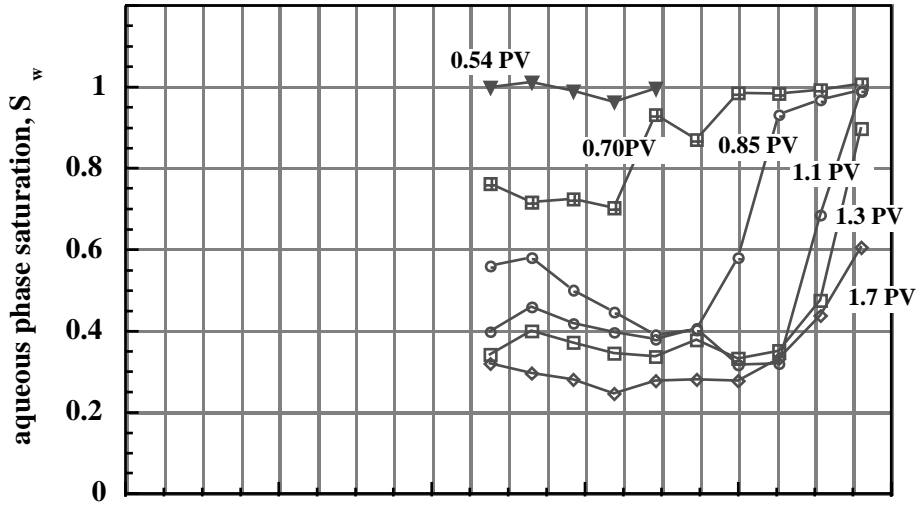
Fig. 32. Transient aqueous phase saturation profiles for displacement with crossflow: (a) sandstone and (b) sand regions. Heterogeneous side injection.

Kovscek et al, 1997) if the effect of gravity is minimal. The striking result is the degree (of displacement in the low permeability sandstone.

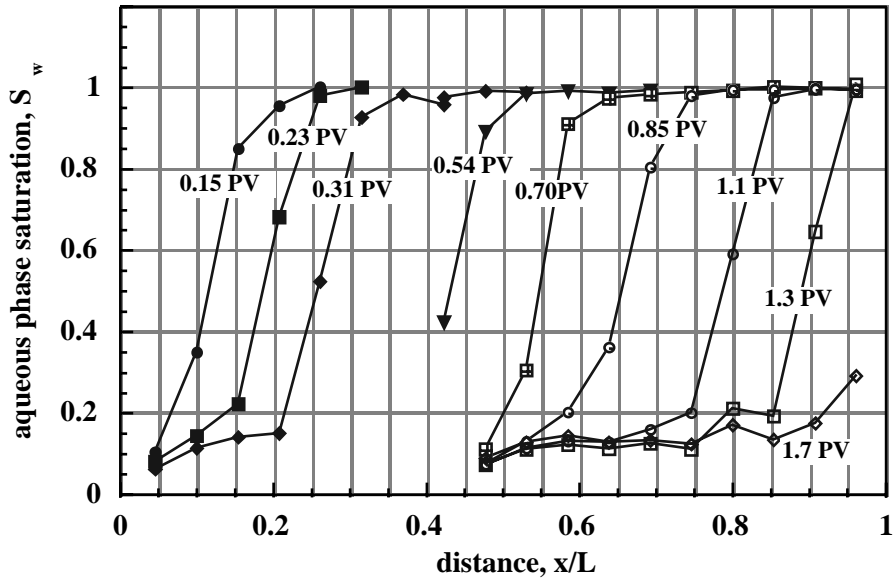
Noncommunicating layers, homogeneous face injection. In this, the third case, gas is injected into the saturated porous medium from the side completely filled with sand. Flow across the cylindrical face of the sandstone is again prohibited by the Teflon jacket barrier.

Figure 33 shows the saturation profiles. In the initial homogeneous section, gas enters the sand, a foam is generated, and displacement of foamer solution from the sand is quite efficient. Foam generation is rapid as a strong displacement front is seen even at 0.15 PV. At roughly 0.54 PV, the foamed gas first enters the sandstone. Again, the foamed gas moves more quickly through the low permeability sandstone than it does through the more permeable sand. The leading edge of the displacement front is at x/L equal to 0.7 in the sandstone and at 0.6 in the sand after 0.7 PV of total gas injection. At 0.85 PV of injection, front positions are roughly 0.85 and 0.75 in the sandstone and sand, respectively. Consistent with this observation, gas breakthrough occurs from the sandstone first.

Initially, foam displacement in the sandstone is not as efficient as in the earlier two cases. Examining the saturation profiles at 0.7, 0.85, and 1.1 PV, we find that the height of the displacement front grows from 0.3 to over 0.6 saturation units.



(a)



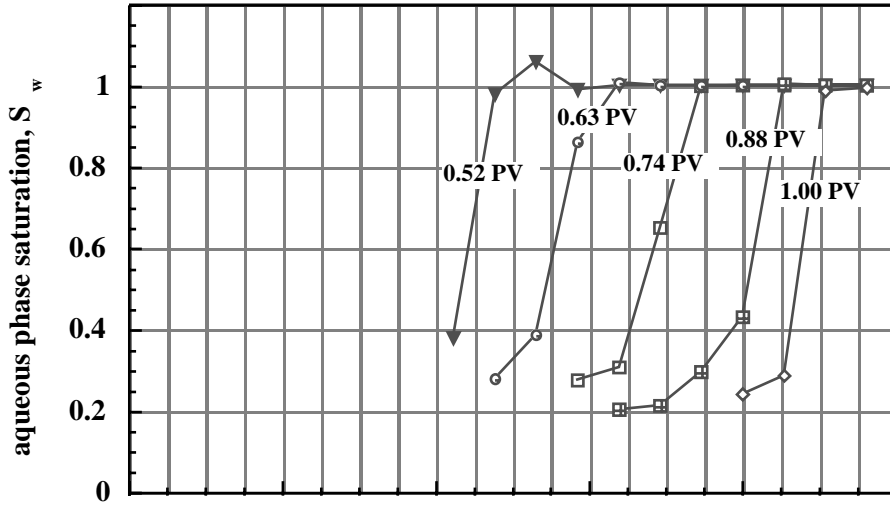
(b)

Fig. 33. Transient aqueous phase saturation profiles for displacement without crossflow: (a) sandstone and (b) sand regions. Homogeneous side injection.

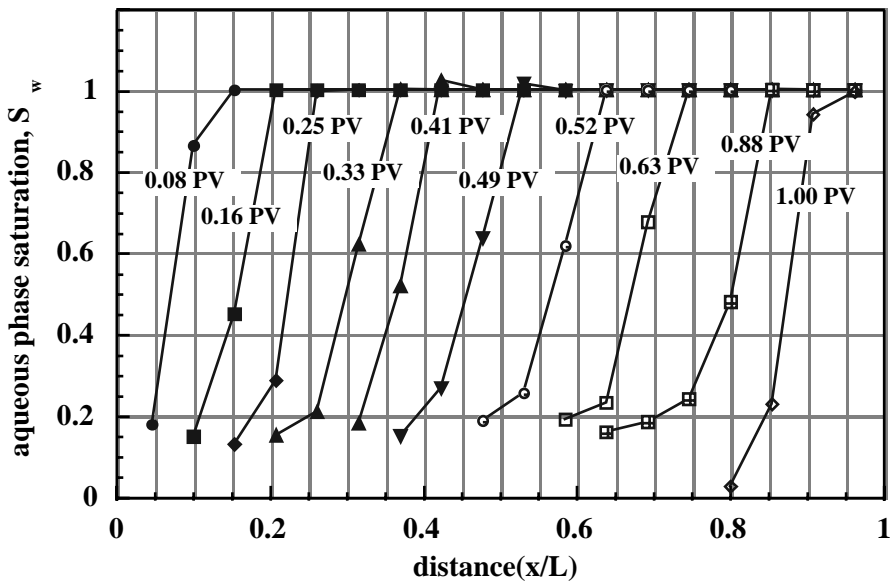
Communicating layers, homogeneous face injection. Figure 34 reports the saturation profiles obtained during gas injection into the homogeneous sand-filled side with capillary communication between the sandstone and sand. Displacement from both the sand and the sandstone is excellent at all time levels. As in the second case where crossflow occurs, saturation fronts move at the same speed in each layer. It is seen by comparing Figs. 34a and 34b that front positions at times of 0.63, 0.74, and 0.88 PV are equal and correspond to x/L equal to 0.65, 0.75, 0.85, respectively.

Discussion

The foam flow behavior discovered in each of these cases can be rationalized by considering foam texture (i.e., bubble size) and the effect that porous medium capillary pressure plays in setting foam texture. It is well established that finely textured foams, that is foams with small average bubble size, present a larger resistance to flow than do coarsely textured foams (Hirasaki *et al*, 1985; Falls *et al*, 1989). In turn, bubble size is dictated by pore-level foam generation and coalescence events (Chambers *et al*, 1991). Foam generation is largely a mechanical process and independent of surfactant formulation and concentration. On the other hand, foam collapse depends strongly on the foamer solution. Foam lamellae are stable provided that surfactant can stabilize the gas-liquid interface against suction capillary pressure that seeks to thin foam films. Hence, it is expected that the rate of foam coalescence increases with porous medium capillary pressure. In turn, the foam becomes more coarse. The characteristic value of capillary pressure that a porous medium approaches during strong foam flow is referred to as the



(a)



(b)

Fig. 34. Transient aqueous phase saturation profiles for displacement with crossflow: (a) sandstone and (b) sand regions. Homogeneous side injection.

limiting capillary pressure, and it is set principally by surfactant type and concentration (Khatib *et al*, 1988).

In the first case reported in Fig. 31, each porous medium accepts whatever portion of the injected gas it desires. Because the sand and sandstone are isolated in the sense that crossflow is not allowed, foam is generated and assumes a texture that is independent of events occurring in the adjacent layers. We surmise that in the low permeability sandstone the foam is not as finely textured as in the sand. Sandstone capillary pressure is larger for a given saturation due to lower medium permeability. Hence, a greater suction pressure is exerted on foam lamellae inducing foam coalescence. This in turn leads to a more coarsely textured foam that is more mobile than its finely textured counterpart in the sand. Hence, foamed gas progresses more rapidly through the low permeability porous media. Nevertheless, gas mobility has been lowered substantially and water displacement is efficient.

In the situation summarized in Fig. 32, the porous media communicate with each other across the long cylindrical interface of the sandstone. Since the porous media communicate, gas at the foam front minimizes its flow resistance via foam bubble texture. When the flow resistance in the sandstone increases, foamed gas diverts into the sand, and vice versa. Thus, foam propagates at an equal rate in each layer because the saturation fronts are bound together by the necessity to maintain the minimum flow resistance. Bubble textures in sand and sandstone are not expected to be identical, but to yield identical gas mobility (Kovscek *et al*, 1997). In this case, the mobility is low and

promotes effective desaturation. In the cases where the heterogeneous section is at the end of the core, similar explanations follow.

When crossflow is prohibited between the sand and the sandstone, each porous medium sets foam texture and, hence, gas mobility independently. Capillary pressure in the low permeability sandstone is higher than in the sand, coalescence ensues, and foam in the sandstone is more mobile than in the sections filled with sand. If crossflow occurs, gas mobility is balanced because low flow resistance forces gas to divert into the adjacent layer. Foam propagates at equal rates in each layer.

Interestingly, the transient experimental results shown here bear striking qualitative similarity to previous simulation of foam behavior in heterogeneous porous media reported elsewhere (Kovscek *et al*, 1997). We note that the preceding qualitative arguments bear strong resemblance to the quantitative results reported in that study.

In conclusion, an experimental study of foam generation and propagation in heterogeneous porous media using Fontainebleau sandstone and Ottawa sand was performed. The contrast in permeability between high and low permeability homogeneous zones was 67 to 1. Despite this drastic permeability contrast and despite the fact that high permeability zones typically lead to gas channeling, foamed gas is diverted to low permeability channels in these experiments. In this regard, the foam generated in these experiments can be regarded as strong. Foam effectively desaturates both the high permeability and low permeability portions of the experimental setup and desaturation is complete following roughly 1 PV of gas injection. This result is found for both systems that permit and prohibit cross flow.

Foam in heterogeneous systems appears to be self regulating in that gas mobilities in each porous medium equalize when layers communicate and nearly equalize in noncommunicating systems. Similar efficient diversion and desaturation is likely in heterogeneous, layered field situations where the permeability contrast is not as large provided that foam is tolerant of the presence of oil. Also, the capillary pressure of each layer must be less than the critical capillary pressure for foam coalescence.

In general, and in agreement with a previous theoretical study, it is observed that when permeability heterogeneities communicate and there is fluid crossflow that foam displacement fronts move at equal velocity in each zone. When crossflow is prohibited by an impermeable barrier, rapid foam propagation and desaturation of the low permeability zone is witnessed.

5. NOMENCLATURE

D_e	Length of widest part of the liquid drop
g	Acceleration due to gravity
H	Tabulated correction factor
N_{CT}	CT number
$N_{CT,AIR}$	Air CT number
$N_{CT,DRY}$	Dry core CT number
$N_{CT,GAS}$	Gas CT number
$N_{CT,MATRIX}$	Matrix CT number
$N_{CT,MEAS}$	Measured CT number
$N_{CT,WET}$	Wet core CT number
$N_{CT,WETPHASE}$	Wetting phase CT number
S_g	Gas Saturation
S_w	Water Saturation

Greek letters

ϕ	Porosity
μ_{WATER}	X-ray attenuation coefficient of water
μ_X	Measured X-ray attenuation coefficient
$\Delta\rho$	Density difference between two fluids
σ	Surface tension

6. REFERENCES

1. Aarra, M.G., Skauge, A., Sognesand, S., and Stenhaug, M., "A Foam Pilot Test Aimed at Reducing Gas Inflow in a Production Well at the Oseberg Field," *Petroleum Geoscience*, **2**, pp. 125-132, 1996.
2. Adamson A. W., "Capillarity," in *Physical Chemistry of Surfaces* edited by John Wiley & Sons, Inc., Canada, pp. 4-48, 1982
3. Aronson, A. S., Bergeron, V., Fagan, M. E., and Radke, C. J., "The Influence of Disjoining Pressure on Foam Stability and Flow in Porous Media," *Colloids and Surfaces A*, **83**, pp. 109-120, 1994.
4. Bond, D. C., and Holbrook, O. C., "Gas Drive Oil recovery Process," U.S. Patent No. 2,866,507, 1958.
5. Bretherton, F. P., *J. Fluid Mech.*, **10**, pp. 166-188, 1961.
6. Burger, J., Personal Communication, Stanford University, Stanford, 1996.
7. Casteel, J. F., and Djabbarah, N. F., "Sweep Improvement in CO₂ Flooding by Use of Foaming Agents," *SPE Reservoir Engineering*, **3** pp. 1186-1192, 1988.
8. Chambers, K. T., and Radke, C. J., *Capillary Phenomena in Foam Flow Through Porous Media*. Interfacial Phenomena in Petroleum Recovery, ed. N.R. Morrow. Vol. Ch. 6. , Marcel Dekker Inc., New York, pp. 191-255, 1991.

9. Chiang, J. C., Sanyal, S. K., Castanier, L. M., Brigham, W. E., and Sufi, A., "Foam as a Mobility Control Agent in steam Injection Processes," paper SPE 8912 presented at the 1980 50th Annual California Regional Meeting, Los Angeles, April, 9-11.
10. Djabbarah, N. F., Weber, S. L., Freeman, D. C., Muscatello, J. A., Ashbaugh, J. P., and Covington, T. E., "Laboratory Design and Field Demonstration of Steam Diversion with Foam," SPE 20067, in Proceedings of the 60th California Regional Meeting, Ventura, April 1990.
11. Falls, A. H., Musters, J. J., and Ratulowski, J., "The Apparent Viscosity of Foams in Homogeneous Beadpacks," *Soc. Pet. Eng. Res. Eng.*, **4**(2) pp. 155-164, 1989.
12. Fergui, O., Quintard, M., Bertin, H., and Defives, D., "Transient Foam Flow in Porous Media: Experiments and Simulations," Proceedings of the 8th European IOR-Symposium, Vienna, Austria, 1995.
13. Fried, A. N., "The Foam Drive Processes for Increasing the Recovery of Oil," No. Report of Investigations 5866, USBM, 1961.
14. Friedmann, F., Chen, W. H., and Gauglitz, P. A.: "Experimental and Simulation Study of High-Temperature Foam Displacement in Porous Media," *Soc. Pet. Eng. Res. Eng.* 6(1), pp. 37-45, 1991.
15. Friedmann, F., Hughes, T. L., Smith, M. E., Hild, G. P., Wilson, A., and Davies, S. N., "Development and Testing of a New Foam-Gel Technology to Improve Conformance of the Rangely-CO₂ Flood," SPE 38837, in Proceedings of the SPE Ann. Tech. Conf. and Exhibition, San Antonio, TX, October 1997.

1. Garg, A., Kovscek, A. R., Nikraves, M., Castanier, L. M., and Patzek, T. W., "CT Scan and Neural Network Technology for Construction of Detailed Distribution of Residual Oil Saturation During Waterflooding," paper SPE 35737 presented at the Western Regional Meeting, Anchorage, Alaska, May 22-24, 1996.
2. Gillis J. V., and Radke, C. J., "A Dual Gas Tracer Technique for Determining Trapped Gas Saturation During Steady Foam Flow in Porous Media," paper SPE 20519 presented at the 65th SPE Annual Technical Conference, New Orleans, LA, September 1990.
3. Hirasaki, G. J., and Lawson, J. B., "Mechanisms of Foam Flow in Porous Media: Apparent viscosity in Smooth Capillaries," *Soc. Pet. Eng. J.*, pp. 176-190, April 1985.
4. Hirasaki, G. J., Miller, C. A., Szafranski, R., Lawson, J. B., and Akiya, N., "Surfactant/Foam Process for Aquifer Remediation," SPE 37257, in Proceedings of the SPE International Symposium on Oil-field Chemistry, Houston, TX, February 1997.
5. Hirasaki, G. J., Miller, C. A., Szafranski, R., Lawson, J. B., Tanzil, D., Jackson, R. E., Londergan, J., and Meinardus, H., "Field Demonstration of the Surfactant/Foam Process for Aquifer Remediation," SPE 39393, in Proceedings of the SPE Ann. Tech. Conf. and Exhibition, San Antonio, TX, October 1997.
6. Hirasaki, G. J., Miller, C.A., Szafranski, R., Tanzil, D., Lawson, J. B., Jackson, R. E., Meinardus, H., Avvakoumides, J., Jin, M., Kennedy, L., Mariner, P., Pope, G. A., and Oolman, T., "AATDF Surfactant/Foam Process for Aquifer Remediation," Report , Intera, Austin, Texas (1997)

7. Hoefner, M. L., Evans, E. M., Buckles, J. J., and Jones, T. A., "CO₂ Foam: Results from Four Developmental Field Trials," SPE/DOE 27787, in Proceedings of the SPE/DOE Ninth Symposium on Improved Oil Recovery, Tulsa, Oklahoma, April 1994.
8. Khatib, Z. I., Hirasaki, G. J., and Falls, A. H., "Effects of Capillary Pressure on Coalescence and Phase Mobilities in Foams Flowing Through Porous Media," *Soc. Pet. Eng. J.*, pp. 919-926, August 1988.
9. Kovscek, A. R., and Radke, C. J., "Fundamentals of Foam Transport in Porous Media", in *Foams in the Petroleum Industry*, L.L. Schramm, Editor., American Chemical Society, Washington, D.C., pp. 115-163, 1994.
10. Kovscek, A. R., Patzek, T. W., and Radke, C. J., "Mechanistic Foam Flow Simulation in Heterogeneous Multidimensional Porous Media," *SPEJ*, **2**(4), pp. 511-526, 1997.
11. Llave, F. M., Chung, F. T.-H., Louvier, R. W., and Hudgins, D. A., "Foams as Mobility Control Agents for Oil Recovery by Gas Displacement," SPE/DOE 20245, in Proceedings of the SPE/DOE Seventh Symposium on Enhanced Oil Recovery, Tulsa, Oklahoma, April 1990.
12. Marsden, S. S., and Khan, S. A., "The Flow of Foam Through Porous Media and Apparent Viscosity measurements," *Soc. Pet. Eng. J.*, pp. 17-25, March 1966.
13. Mohammadi, S. S., Van Slyke, D. C., and Ganong, B. L., "Steam-Foam Pilot Project in Dome-Tumbador, Midway-Sunset Field," *SPE Reservoir Engineering*, **4**(1), pp. 7-16, 1989.
14. Patzek, T. W., and Koinis M. T., "Kern River Steam-Foam Pilots," *Journal of Petroleum Technology*, **42**(4), pp. 496-503, 1990.

15. Robin, M., "Laboratory Evaluation of Foaming Additives Used to Improve Steam Efficiency," SPE 16729, in Proceedings of the 62nd Annual Technical Conference and Exhibition of the Society of Petroleum Engineers, Dallas, September 1987.